Institute of Robotics and Intelligent Systems

Technische Universität Wien

Institute for Regenerative Medicine • IREM

DIPLOMARBEIT

Design and Development of an Automated Device for the Seeding of Tissue-engineered Vascular Grafts

Ausgeführt am

Institute for Regenerative Medicine (IREM), University of Zurich

unter der Anleitung von

Dr. Sarah E. Motta

Dr. Simone Gervasoni

Prof. Dr. med. S. P. Hoerstrup, PhD

Prof. Dr. med. M. Y. Emmert, MD, PhD

with the support of

Univ. Prof. Dipl.-Ing. Dr. mont. Jürgen Stampfl

durch

Alireza Vasfi

May 2021

Acknowledgments

I would like to thank Prof. dr. med. S. P. Hoerstrup and Prof. dr. med. M. Y. Emmert for giving me the opportunity to work on my master's thesis under their supervision and guidance. I would also like to thank Univ.Prof. dipl.-ing. dr. mont. Stampfl for all of his help and support.

Special thanks to Dr. Sarah Motta for teaching me about tissue-engineered medicine and for her help and time during my research work.

Furthermore, I would like to thank Dr. Simone Gervasoni for his technical advice.

A big thank you also goes to all of my colleagues at the working group for their help and insight.

Contents

Abstract

Vascular bypass aims at restoring normal blood circulation in cardiovascular diseases affecting blood vessels. Currently used vascular prostheses, such as autologous vessels or non-biodegradable polymeric conduits suffer of several limitations, like limited availability, poor quality, low patency, thrombotic occlusion etc. Hence, the generation of tissue-engineered vascular grafts (TEVGs) with similar structural and mechanical properties to those of native blood vessels represents a hot topic in the field of cardiovascular regenerative medicine. This approach allows the construction of TEVGs using scaffolds, cells and a bioreactor. The scaffold material as well as the cell type used for seeding the scaffold play an important role in determining the properties of a TEVG. In fact, cells and their seeding lead to a precise ECM production and composition, which will then affect the mechanical properties as well as graft remodeling potential upon implantation. In this study, we assessed the feasibility to produce an automated cell seeding device, designed manufactured to guarantee uniformity, efficiency, and reproducibility of user-independent cell seeding technique. in comparison to other seeding approaches, this method will allow for a homogeneous cell distribution onto the grafts and avoid the cell being suspended for a long period and potential subsequent detrimental effects.

Zusammenfassung

Der vaskuläre Bypass zielt darauf ab, die normale Blutzirkulation bei Herz-Kreislauf-Erkrankungen, welche die Blutgefäße betreffen, wiederherzustellen. Gegenwärtig verwendete Gefäßprothesen, wie autologe Gefäße oder nicht biologisch abbaubare Polymerstrukturen, leiden unter mehreren Einschränkungen, wie begrenzte Verfügbarkeit, schlechte Qualität, geringe Durchgängigkeit, thrombotischer Verschluss usw. Daher ist die Herstellung von regenerativ hergestellten Gefäßtransplantaten (TEVGs) mit ähnlichen strukturellen und mechanischen Eigenschaften wie native Blutgefäße ein vielversprechender Ansatz im Bereich der kardiovaskulären regenerativen Medizin. Dieser ermöglicht die Konstruktion von TEVGs unter Verwendung von Transplantgerüsten, Zellen und einem Bioreaktor. Das Material des Transplantgerüsts sowie der Zelltyp, der für das Ansetzen der Zellkultur in diesem verwendet wird, spielen eine wichtige Rolle bei der Bestimmung der Eigenschaften eines TEVG. Tatsächlich führen Zellen und deren Kultivierung zu einer präzisen ECM-Produktion und -Zusammensetzung, die dann die mechanischen Eigenschaften sowie das Potenzial für das Transplantat-Remodeling bei der Implantation beeinflusst. In dieser Studie haben wir die Machbarkeit einer automatisierten Vorrichtung für das Ansetzen von Zellen bewertet, die so konstruiert ist, dass sie die Einheitlichkeit, Effizienz und Reproduzierbarkeit der benutzerunabhängigen Kultivierungstechnik garantiert. Im Vergleich zu anderen

Kultivierungsansätzen ermöglicht diese Methode eine homogene Zellverteilung auf den Transplantaten und vermeidet eine Zellsuspension sowie mögliche nachteilige Auswirkungen.

Nomenclature

Abbreviations

CAD	Computer-aided design
CHD	Coronary heart disease
DOF	Degree Of Freedom
DMLS	Direct Metal Laser Sintering
EC	Endothelial cell
ECM	Extracellular matrix
e-PTFE	expanded Polytetrafluoroethylene
FDM	Fused deposition modeling
hDFB	Human dermal fibroblast
MJF	Multi Jet Fusion
PCB	Printed Circuit Board
PET	Polyethylene terephthalate
PAD	Peripheral arterial disease
PLA	Polylactic acid
PGA	Polyglycolic acid
RAS	Renal artery stenosis
SMC	Smooth muscle cells
SV	Saphenous vein
SLA	Stereolithography
SLS	Selective Laser Sintering
TEVG	Tissue Engineered Vascular Graft

1. Introduction

Cardiovascular disease is the leading cause of death worldwide (1), and it is expected to rise to a yearly death toll of 23.3 million people by 2030 (2). A synthetic vascular graft mostly made from non-biodegradable materials such as polyethylene terephthalate (PET, Dacron) or expanded polytetrafluoroethylene (e-PTFE) may be utilized to bypass or replace a damaged or occluded vessel (3). Despite, these grafts have proven satisfactory long-term results, synthetic materials are not clinically optimal due to the inability of mimicking the elastomechanical characteristics of the native arterial tissue, increased risk of calcification, thrombosis, stenosis, and infection while lacking in growth potential and durability (4).

To overcome the limitations associated with synthetic graft and limited autologous transplantation, tissue-engineered vascular grafts (TEVGs) with the ability to remodel, grow and repair have been proposed as an attractive potential solution to the problems of currently-adopted grafts (5).

1.1. Cardiovascular system and diseases

The cardiovascular system permits blood to circulate throughout the body and in particular, from and to the heart, the tissues, and the organs. Arteries transport oxygen and nutrients to the tissues, while veins remove carbon dioxide and waste products of metabolism from the tissues. However, the opposite is true for the pulmonary circulation, where the arteries transport deoxygenated blood from the right ventricle to the lungs, and the veins carry oxygenated blood toward the left atrium. The key components of the human cardiovascular system are the heart, blood vessels, and blood (6).

There are five types of blood vessels in the human body: the arteries, the arterioles, the capillaries, the venules, and the veins. The arteries and veins have 3 layers: the intima, the media, and the adventitia. The intima is the innermost layer and it is the thinnest layer formed by a monolayer of endothelial cells. The tunica media is the middle layer, it is thicker in the arteries than it is in the veins. Finally, the outermost layer of a blood vessel is tunica adventitia that is the thickest layer in the arteries and veins. There are various cardiovascular diseases involving the blood vessels, which often require surgery. These might include aortic aneurysm, renal artery stenosis, coronary artery disease, and peripheral arterial disease. Aortic aneurysm or dilation of the aorta causes weakness in the aorta and consequently, the risk of aortic rupture would increase. Rupturing the aorta may lead to shock and death due to massive internal bleeding (7). Renal artery stenosis (RAS) is the narrowing of renal arteries. Fibromuscular dysplasia or atherosclerosis most often are the causes of RAS. The narrowing of renal arteries may impede

blood flow to the kidneys, resulting in decreased kidney function and renovascular hypertension (8,9). Coronary heart disease (CHD) causes an inadequate blood flow and oxygen to the myocardium due to the build-up of atherosclerosis in the coronaries (Figure 1). CHD is the most common cardiovascular disease and the main cause of death worldwide (10). Peripheral arterial disease (PAD) is a chronic disease of blood vessels that supply blood to the arms and legs and is caused by atherosclerosis. Patients with PAD are at high risk for all-cause mortality. PAD mostly affects the lower limbs, iliac arteries, and abdominal aorta (11).

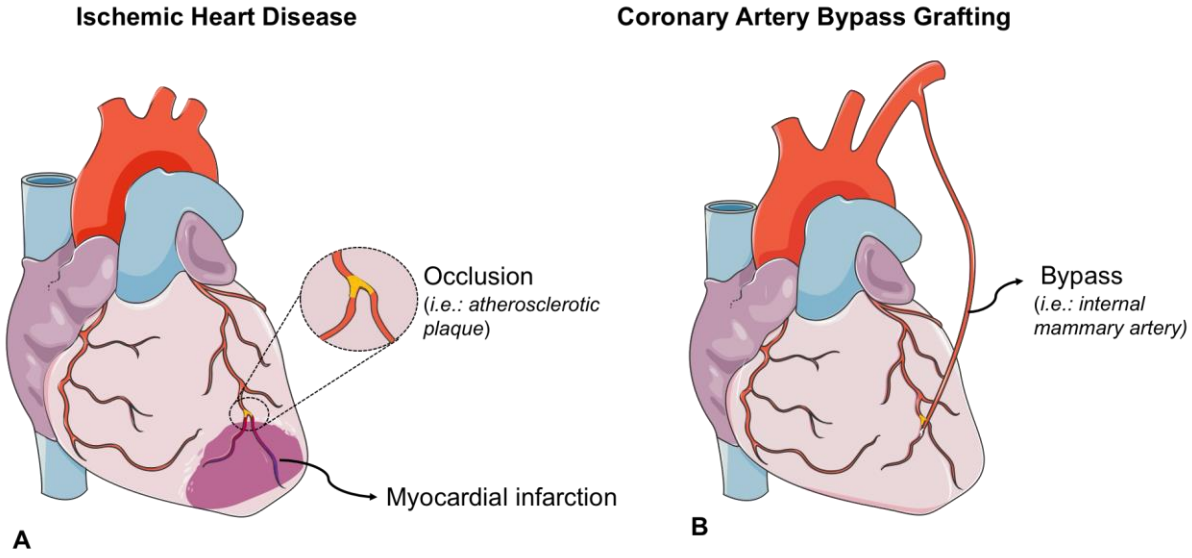

Figure 1: Schematic representation of ischemic heart disease and current treatment option. A) coronary artery occlusion by an atherosclerotic plaque can significantly limit the blood flow to the heart muscle, creating an infarcted area in the myocardium. **B)** the current gold-standard treatment option is to overcome the occlusion by performing a bypass grafting using an autologous vessel, such as the internal mammary artery (Source: Fioretta ES. Et al., Tissue-Engineered Vascular Grafts, Springer, 2019).

1.2. Current clinically-available vascular substitutes

Nowadays, synthetic polytetrafluoroethylene (PTFE or Gore-Tex) and polyethylene terephthalate (Dacron) conduits are the most widely used vascular graft replacements. Like the native blood vessels, the third generation of ascending aorta Dacron grafts have three layers, the inner layer is a standard uncoated woven Dacron graft that is in contact with blood, a standard expanded polytetrafluoroethylene graft is the outer layer, and eventually, to have a three-layer structure of the triplex vascular graft by a central layer of self-sealing elastomeric membrane these two layers are fused together (12).

Over the last 50 years, vascular prostheses have demonstrated good performance, however, such prostheses are prone to failure due to poor mechanical and regenerative properties. In fact,

synthetic grafts are not able to mimic the mechanical characteristics of the native arterial tissue, and consequently, the lack of adequate compliance lead to para-anastomotic pseudoaneurysm, aneurysm or dilation, and mechanical failure, resulting in aberrant cell signaling, maladaptive remodeling and significant morbidity in the patients (13-15). Several studies have revealed that in respect to native arteries currently-available vascular grafts exhibit more than four times reduced compliance ($8 \times 10{-}2$ % versus $1.8 \times 10{-}2$ % mmHg−1) (16). In addition, when synthetic material is inserted into the arterial system, it reflects in thrombosis and endothelial dysfunction (17-19).

Currently, the gold standard material for vascular grafting is the patient's own artery or vein. Saphenous vein (SV) is the most commonly used autologous graft, due to the limited availability of arteries, such as the radial artery or internal thoracic artery, and the great complexity associated with their removal (20-23). Patency rates for SV grafting remain limited with both femoropopliteal and coronary bypass grafts exhibiting failure rates of about 50% at 10 years (24,25). Furthermore, autologous vessels may be unsuitable for use due to poor quality and may cause donor site morbidity (26-28). In the affected patient population, either for reasons of use in previous operation or anatomy there is not sufficient amount of native tissue. Given the limitations of current autologous and synthetic graft replacements, a long-term solution with regenerative, self-repair, and growth capacity is required. (29)

1.3. Vascular Tissue engineering

Tissue engineering is a scientific field born over 20 years ago as a potential solution to the drawbacks of clinically-available prostheses. A TEVG must withstand the pressure exerted by the flow of blood without experiencing permanent deformation through aneurysm (i.e. burst pressure) (14,30). It needs to be biocompatible, thrombus resistant, and non-immunogenic. To prevent high stresses around the anastomosis, the graft ought to possess suitable compliance and a physiological geometry to reduce the associated risk of failure (31-35). Most importantly, the graft should be able to remodel, grow, and self-repair in vivo, and to endure the hemodynamic changes with sufficient mechanical properties (36). Furthermore, from a clinical perspective, a TEVG should be cost-effective, logistically convenient to manipulate, and readily available. Cells, scaffolds, and bioreactors are the three components that are essential and interdependent to each other when endeavoring to form organized neotissue. The construct of newly created neotissue would theoretically be less prone to infection, thrombo-resistant, and have growth capacity since is composed of autologous tissue. A TEVG with the ability to remodel, repair and grow in vivo while autograft surgery is not needed has clear advantages particularly for young patients, and would be of great benefits.

Over the past decades, several tissue engineering strategies to create the suitable TEVG were designed. Classical in-vitro tissue engineering approaches adopt the seeding of a relevant cell type, such as fibroblasts, smooth muscle cells (SMCs), or mesenchymal stem cells (MCSs) in a temporary scaffold (Figure 2). Afterward, the construct is cultured in vitro, while the cells

produce their own extracellular matrix (ECM) the scaffold materials are degraded. The mechanical strength, essential to maintain vessel function and structure, is provided by this cell-produced ECM, particularly collagen. During the culture period in vitro various mechanical and biochemical stimuli are employed to assess the maturation process (37-40). Although these approaches vary considerably in terms of cell source, materials, culture protocol, and manufacturing methods, they can be mainly categorized into three methods, scaffold-based methods using natural or synthetic materials, self-assembly processes, and decellularized natural matrix techniques.

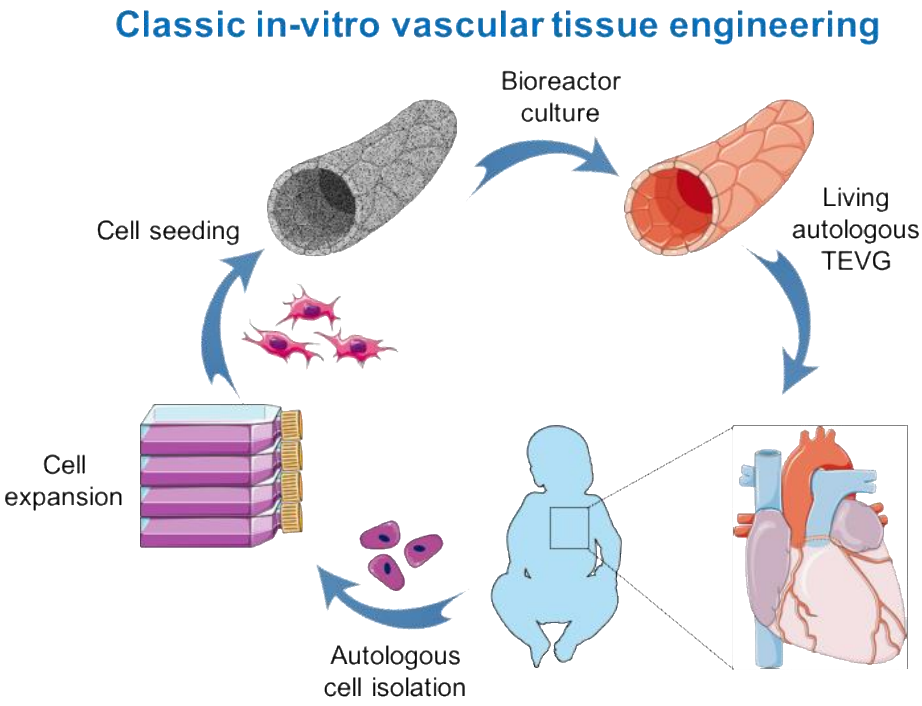

Figure 2: Schematic representation of the classic in-vitro vascular tissue engineering. This approach aims at the development of an autologous TEVG by isolating (vascular or stem) cells from the patient. The cells are expanded, seeded onto a biodegradable porous scaffold, and cultured in the presence of chemical and mechanical cues (provided by the culture medium and bioreacotr system) to favour extracellular matrix deposition. After a predetermined culture period, the graft is ready for implantation into the patient (Source: Fioretta ES. Et al., Tissue-Engineered Vascular Grafts, Springer, 2019).

In situ approaches have also been studied to bypass these complex in vitro processes. Here, the scaffolds can be of synthetic nature or biological and are directly implanted with or without cells in the body of the host. Host cells grow and migrate within the newly implanted construct, which is expected to self-repair, grow, and remodel. In this approach, the implanted engineered construct is not functionally mature, and the body is used as a bioreactor to regenerate the tissue.

In situ tissue engineering is proposed as an on-the-fly and cost-effective approach, using off-the-shelf and logistically simple grafts (41,42).

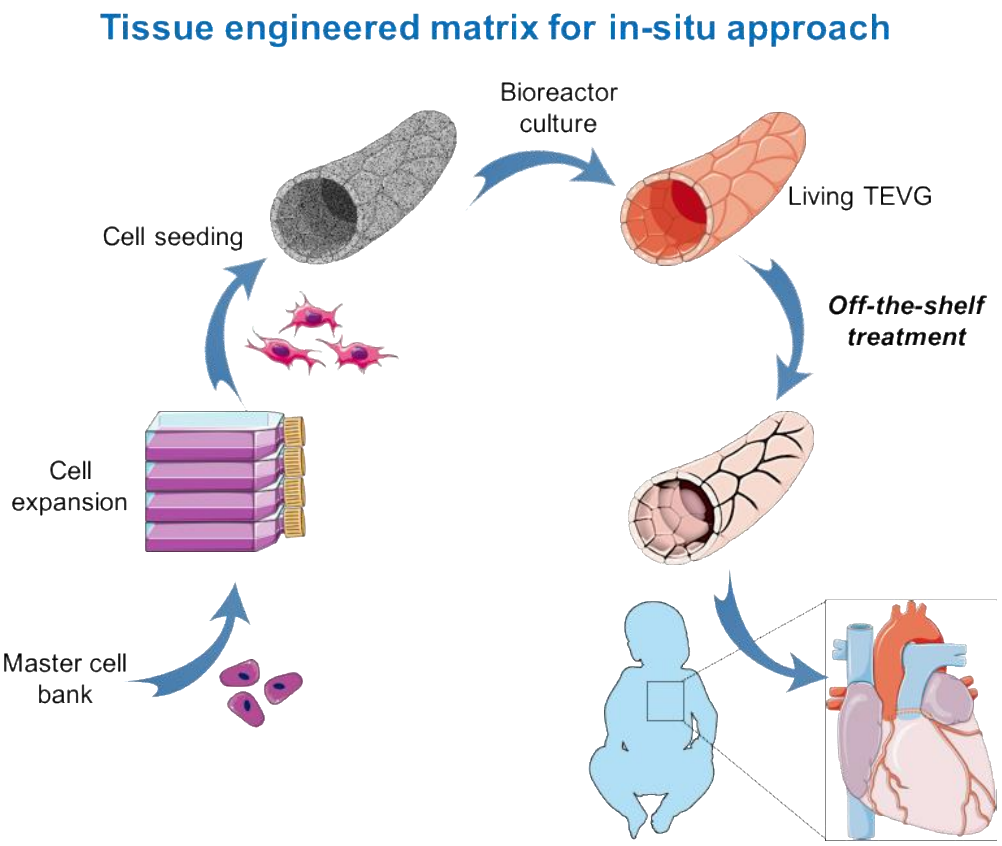

Figure 3: Schematic representation of the in-situ vascular tissue engineering approach using a tissue engineered matrix (TEM). TEM-based scaffolds consist of an in-vitro grown extracellular matrix depleted of cells that is obtained following the classic tissue engineering methodologies. Briefly, allogenic cells are used to produce an in-vitro TEVG. After culture, the graft is decellularized to ensure off-the-shelf availability and immunocompatibility of the product. The graft can then be implanted into the patient where in-situ tissue regeneration will occur. (Source: Fioretta ES. Et al., Tissue-Engineered Vascular Grafts, Springer, 2019)

1.4. Scaffolds for TEVGs

Scaffold materials are necessary to allow cell attachment, provide initial mechanical support and define the vessel geometry. One fundamental aspect of scaffold materials is their in-vivo degradation rate. To this extent, the properties of various natural and synthetic polymers have been evaluated. Upon implantation, the scaffold should be degraded and replaced at a rate that balances with the rate of ECM production by the host cells. First, polymers experience a loss of mechanical properties due to the degradation via hydrolysis followed by a decrease in mass to volume ratio. The degradation rate of these polymer materials depends on their exposed surface

area, initial molecular weight, and physical state (43). To design a TEVG, an important first step is choosing a suitable material with ideal mechanical properties, immunogenicity, and rate of degradation. Many techniques and materials have been investigated for the construction of the grafts such as Polyglycolic acid (PGA), Poly-L-lactic acid (PLLA), decellularized matrices, collagen sheets, and hydrogels. PGA, Polyglycerol sebacate (PGS), Polylactic acid (PLA), and Poly-ε-caprolactone (PCL) are the most commonly used biodegradable scaffolds.

Due to the lack of bio-activity of synthetic scaffolds, natural polymers have been investigated as an alternative option. These polymers exhibit excellent biological performances, furthermore, they do not cause toxicity or chronic inflammation (44). Fibrin, collagen, elastin, gelatin, and silk fibroin are the most widely used natural polymers in tissue engineering. Outstanding successes have been achieved using fibrin as a scaffold material. Fibrin is an insoluble body protein involved in tissue repair and wound healing (45,46). The fibrin clot provides structural support for proliferation, adhesion, and migration of the cells involved in the tissue repair and healing and is obtained by fibrinogen polymerization due to the addition of thrombin (47,48). Collagen as the main ECM protein in the body exhibits excellent biological properties, biocompatibility, low antigenicity, biodegradability, and low inflammatory response (45,46,49). Collagen type I is mainly used as a scaffold for application in vascular tissue engineering (45). Elastin as the main ECM in the arterial wall confers resilience, elastic recoil, and durability (50-52). Elastin is an autocrine regulator to endothelial cell (EC) and SMC activity, it inhibits proliferation and migration of SMCs and improving proliferation and attachment of ECs (50,52). Gelatin is a collagen derivative, obtained by denaturing the triple-helix structure of collagen. Due to exhibiting similar biocompatibility, mechanical properties, and biodegradation with collagen, gelatin has become a noteworthy polymer for TEVG application. Furthermore, a gelatin TEVG shows better biocompatibility, antithrombogenicity, and biointegration than a non-gelatin TEVG (53-55). Silk-derived fibroin offers excellent biocompatibility and mechanical properties, furthermore, it degrades slowly in vivo and absorbs as a biocompatible amino acid. Silk fibroin can be built into various materials such as porous sponges, fibers, and knitted scaffolds (56).

Natural polymers exhibit reduced mechanical strength compared to synthetic polymers and are more susceptible to degradation, which may lead to rupture and aneurysm formation if not carefully controlled. Generally, prior to in vivo implantation natural polymers are seeded and cultured with cells in vitro to acquire a partial remodeling of the construction, which leads to improving the mechanical properties of the graft. In an effort to improve cell adhesion and biocompatibility, a combination of both natural and synthetic polymers has been proposed (57) .

Hybrid scaffolds are a combination of superior biological behavior of natural polymers with sufficient mechanical properties of synthetic polymers. Hybrid scaffolds are biological-based scaffold materials that enhance cellular infiltration and biocompatibility and reduce the possibility of a foreign body reaction by incorporating fibrin, collagen, elastin, and/or gelatin. Often the mechanical properties, specifically, in terms of burst pressure (485 ± 25 mmHg) and ultimate tensile strength (0.34 ± 0.14MPa), and biodegradation profiles are less than optimal, therefore, they are chemically modified or combined with biodegradable synthetic polymers.

Furthermore, the structural integrity of graft can be improved by naturally occurring polymers such as silk and chitosan (57).

Another technique to incorporate the strength of natural tissue ECM into a scaffold is the use of decellularized natural matrices. Decellularization takes advantage of the mechanical performance and structure of naturally occurring ECM while minimizing any adverse immunological reaction by removing all cellular and antigenic components of the tissue (58-60). After removing antigenic components, while mechanical properties and structural integrity of the ECM are preserved, this theoretically intact ECM can be used as a scaffold to support cell attachment and growth. The decellularization process usually involves a variety of physical methods, such as pressure, agitation, and abrasion, biological agents, such as chelating agents and enzymes, and chemical agents, such as detergents and solvents, acids and bases (43). The advantages of decellularized matrices are correlated to their structural and functional proteins, fundamental for cell differentiation, migration, proliferation, and adhesion (43,61). Insufficient decellularization may lead to adverse immune reactions and eventually, sudden failures in implants, while important ECM components may be removed with aggressive treatments, leading to altered mechanical properties (62-65).

A complete biological TEVGs without the need of supporting matrix or a scaffold has been investigated. This approach avoids issues that are due to synthetic materials, including infection, inflammation, and stenosis, allowing for the improvement of the patency rate and complete graft integration (46,66). Sheet-based tissue engineering, cell printing, and microtissue aggregation are the three main approaches that have been developed to creating TEVGs without the use of scaffolds. The sheet-based tissue engineering process involves the production of 2D cell sheets which are cultured and then shaped around a mandrel, forming the tubular structure that is matured into a TEVG. For the fabricating of TEVGs by self-assembly of microtissues, cell aggregates are placed in a mold and then combined to form a TEVG. In the bioprinting TEVG approach, supporting material and cells are precisely deposited and fused in a layer-by-layer manner, to develop a 3D construct (66-68).

1.5. Cell sources for TEVGs

An ideal cell source for TEVGs should be easily available and conveniently expanded in vitro, and in the case of autologous cells, they must be obtained in a minimally invasive manner. For cardiovascular tissue engineering, the capability of the cells to produce and assemble ECM components such as elastin and collagen are essential (69,70). Relevant autologous adult vascular cells, such as fibroblast, ECs, and SMCs are important for creating a stable TEVG. SMCs and ECs are the main components of the media and intima of a blood vessel, respectively. By seeding mononuclear cells on a biodegradable graft, rapid intima formation is promoted and exhibits physiological properties similar to human blood vessels (71). However, the hyperproliferation of SMCs should be controlled to prevent neointimal hyperplasia. ECs synthesize numerous important growth factors and regulators, furthermore, they are responsible

for numerous physiological functions (72). A confluent EC monolayer on all surfaces of the luminal of a TEVG can be established to confer resistance to thrombosis and hyperplasia. Due to the limitations of the autologous adult cells for vascular tissue engineering, several stem cell sources, including MSCs, bone marrow mononuclear cells, progenitor cells, adipose tissue stem cells, hair follicle stem cells, muscle-derived stem cells, and induced pluripotent stem cells, have been investigated (72).

1.6. Cell seeding techniques

Several TEVGs are in preclinical development stages or in clinical trials around the world. The translation of TEVG technologies from the bench to the clinical is examined intensively by regulatory agencies, and over the past three decades, researchers have been working to optimize the efficiency and safety of these products. Seeding methods used to develop a TEVG is one of the areas of intensive investigation (73-78).

Cell seeding is a critical step in vascular tissue engineering due to its influence on cell attachment efficiency, differentiation and growth. Numerous seeding techniques have been developed in the last decades, however, many of these have limited clinical applicability due to scarce reproducibility and time-consuming procedures (79,80). Cell seeding techniques should allow highly efficient, rapid, uniform, user-independent, and reproducible results to guarantee clinical applicability. These strategies are classified into two main categories, passive and active seeding, and will be discussed in the next sections.

1.7. Passive seeding

Passive seeding is the simplest available method and results in high cell viability. However, these manual procedures are the least efficient approach and fail in achieving reproducibility and uniformity (89). In brief, these methods involve the manual pipetting of cell suspensions directly on top of the scaffold or into the lumen of the graft and over time infiltrate the porous structure. After pipetting of the concentrated cell suspension, the construct is incubated, and finally placed in a petri dish with cell medium. To optimize seeding efficiency, statically seeded cells can be incubated for up to several days. The passive seeding technique results in a seeding efficiency of about 10%-25% (81), which can be increased with longer incubation times (82).

A scaffold can be functionalized with active molecules or biological adhesives such as fibronectin and fibrin to mimic native ECM and to facilitate cells attachment or to entrap them in situ (83). Currently, fibronectin is the most commonly used protein but other adhesive coatings such as collagen, fibrin, plasma, and laminin have also been investigated (77,84).

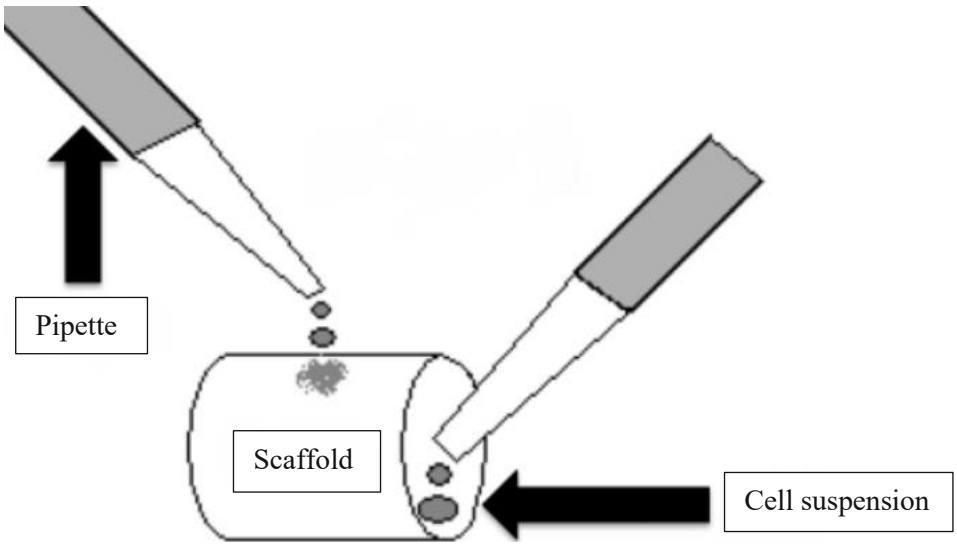

Figure 4: Passive seeding

1.8. Active seeding (Dynamic seeding)

The active seeding method uses single or multiple external driving forces to increase uniformity, cell seeding efficiency, infiltration in the scaffold, and decrease logistical complexity. Rotational and vacuum seeding are the two mostly adopted methods (78, 85,86).

1.8.1. Rotational systems

Rotational seeding exploits the hydrostatic forces by placing a graft in a spinner flask with medium or cell suspension. Here, the cells are driven onto the scaffold by the rotation of the medium. 0.2 up to 500 rpm is the seeding conditions range with a culture period from 12 hours up to 72 hours. 2500 rpm has been indicated to increase graft wall penetration and seeding efficiency (87). However, cell viability is maintained in centrifugal seeding, such high-speed rotation may affect cell morphology. On the contrary, the low-speed rotation has shown no effect on cell morphology, however it increases the seeding times required and may lead to reduced seeding efficiency at lower concentrations (88). Furthermore, this relatively long seeding period is not suitable for the one-day seeding and implanting procedure.

1.8.2. Vacuum seeding

Vacuum seeding exploits the internal pressure or external vacuum pressure force by which a cell suspension travels through the micropores of the scaffold either due to external vacuum or internal pressure (89). Despite this simple and rapid method shows high efficiency, the culture period is time-consuming, furthermore, it might exhibit adverse effects on cell viability and morphology when using this approach in vivo (89).

1.8.3. Magnetic cell seeding

In this method, the magnetic force is used to increase cell-seeding efficiency. The fundamental principle of this method is attracting nanoparticles inside of seeded cells by using magnetic forces (90). Despite, this technique is fast and simple with high seeding efficiency, it might have an adverse effect on cell morphology, cell viability, and cell proliferation. Furthermore, the fate of these nanoparticles once the cells are replaced is still under investigation (91-93).

1.8.4. Electrostatic cell seeding

Here ECs maturation and adhesion are enhanced with the temporary induction of a positive charge on an otherwise negatively charged graft luminal surface. In this method the electrostatic properties of scaffolds are manipulated with the aim of obviating the morphological maturation before and cell retention after implantation, which are the two major limitations of EC seeding. Although this method is fast and has high seeding efficiency, it can only be used for ECs, additionally, long term adverse effects are unknown (94,95).

1.8.5. Perfusion bioreactor system

This method can be used to mimic biomechanical stresses and physiological conditions that cells and vessels are exposed to in vivo such as hydrostatic pressures, cyclic stretch, and fluid shear stresses to promote ECM formation and cellular adhesion and differentiation (75,96,97). This technique has the advantage to promote morphological cell maturation and has good seeding efficiency. However, it is quite a complex procedure which increases the risk of contamination (98,99).

1.8.6. Photopolymerized hydrogels for seeding

In this method, derivatives of photopolymerizable polyethylene glycol are used to mimic the ECM properties (100). Without any adverse effects, this technology can be utilized in direct contact with tissues and cells. Although this method exhibits promising results in vitro regarding cell proliferation, viability, and seeding, there are still concerns regarding the suitability of the

hydrogel mechanical properties as well as its thrombogenicity potential and resistance to venous and/or arterial pressures (100,101).

1.8.7. Hybrid systems

Hybrid techniques refer to multiple seeding systems that are combined, such as vacuum and bioreactor systems, pressure differential system, rotational systems (102), or combinations of other methods (103).

A broad spectrum of techniques has been investigated to achieve higher seeding homogeneity and efficiency. However, they exhibit several drawbacks such as time-consuming procedure, complexity, adverse shear-stress on cells, cells washout, and poor cell uniformity. Therefore, to overcome such limitations, in this study we propose a novel automated cell seeding device for TEVGs.

1.9. Aim

The aim of the study is the design and development of an automated device for the seeding of TEVGs. Cell seeding significantly affects cell differentiation and growth within the scaffold and the consequent success or failure of the prosthesis. The manual seeding of cells by pipetting onto a biodegradable scaffold is an effective method of cell seeding and preclinical experiences substantiated the remodeling and growth capacities of TEVGs. Their large-scale translation into clinical practice is however hindered by the use of operator-dependent manufacturing processes, including manual seeding procedures. To achieve clinical applicability cell seeding techniques must allow user-independent, highly efficient, reproducible, uniform, and rapid cell seeding. We here propose the seeding method's automation. The seeding will therefore be completely operator-independent and will achieve uniform and homogeneous cell distribution. The current study takes advantage of both active and passive seeding to propose a simple, cost- and time-efficient technique that is applicable to any cell type, scaffold material, length from 6cm up to 10 cm, and diameter from 1mm up to 20mm, furthermore this method will allow reproducible and controlled TEVG production and can be used in the clinical setting.

After an introductory chapter on the different TEVG techniques and the state-of-the-art, chapter 2 reports the device manufacturing. Here, the experimental goals consisted into 1) design the individual components and assemble the seeding device using a computer-aided design (CAD) software; 2) identify their mutual interactions; 3) build a device prototype compatible with laminar flow hoods applications (sterile conditions). Chapter 3 illustrates the automated cell-seeding device electronics and chapter 4 reports the code delivery for programming and controlling the automated device. In chapter 5 we talk about the methods and proof-of-concept results, finally after the discussion in chapter 5, in chapter 6 we summarize and briefly discuss the future development of the device. Furthermore, a sample of the G-codes written for the

device can be found in the appendix. This G-code illustrates seeding the 18 strip lines of the human dermal fibroblast cells onto the scaffold.

2. Cell seeding device mechanics

2.1. Concept

The initial idea of the first device prototype took inspiration from fused deposition modeling (FDM) 3D printers. The dynamic model of the FDM printer has three Degrees Of Freedom (DOF), consequently, there are three stepper motors for the movements. To allow the simultaneous x, y, z, movement and the rotation of the graft in the cell seeding device, we here implemented a fourth DOF.

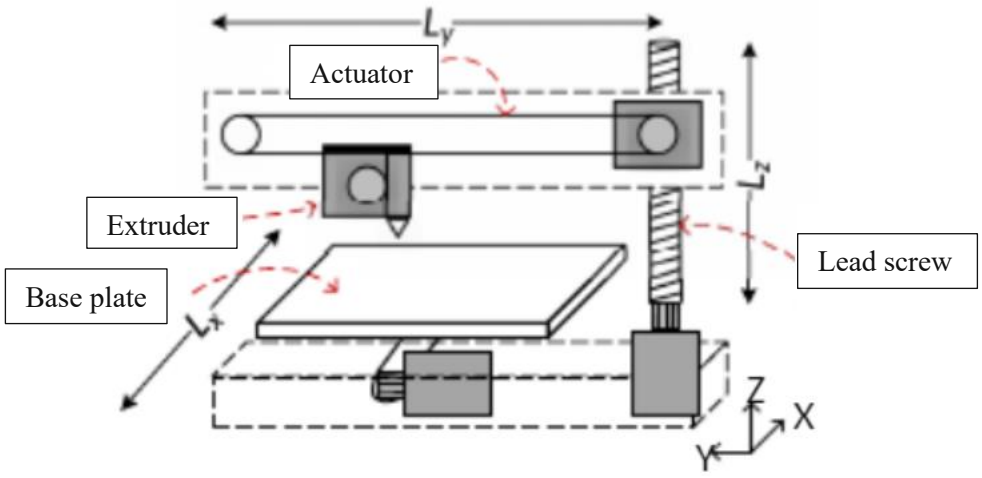

Figure 5: Simplified mechanical structure of FDM

As it is shown in figure 5, the mechanical structure of an FDM consists of a base plate, lead screw, actuator, and extruder, which can be moved in x and y-directions. The cell seeding device is designed based on the graft dimension, the length of the graft is 70 mm, and the diameter of 16 mm. To fix the graft properly in its position, we implemented an adjustable holder which can accommodate the seeding of grafts of variable dimensions (lengths and diameters). In the device can now be fitted grafts with any length from 60 mm up to 100 mm and any diameter from 1 mm up to 20 mm.

2.2. CAD design

The design process started with the drawing of the device in CAD Solidworks 2020 taking inspiration from the main structure of a FDM 3D printer and its X and Y axes. Figures 6 and 7 illustrate the CAD design with Solidworks 2020.

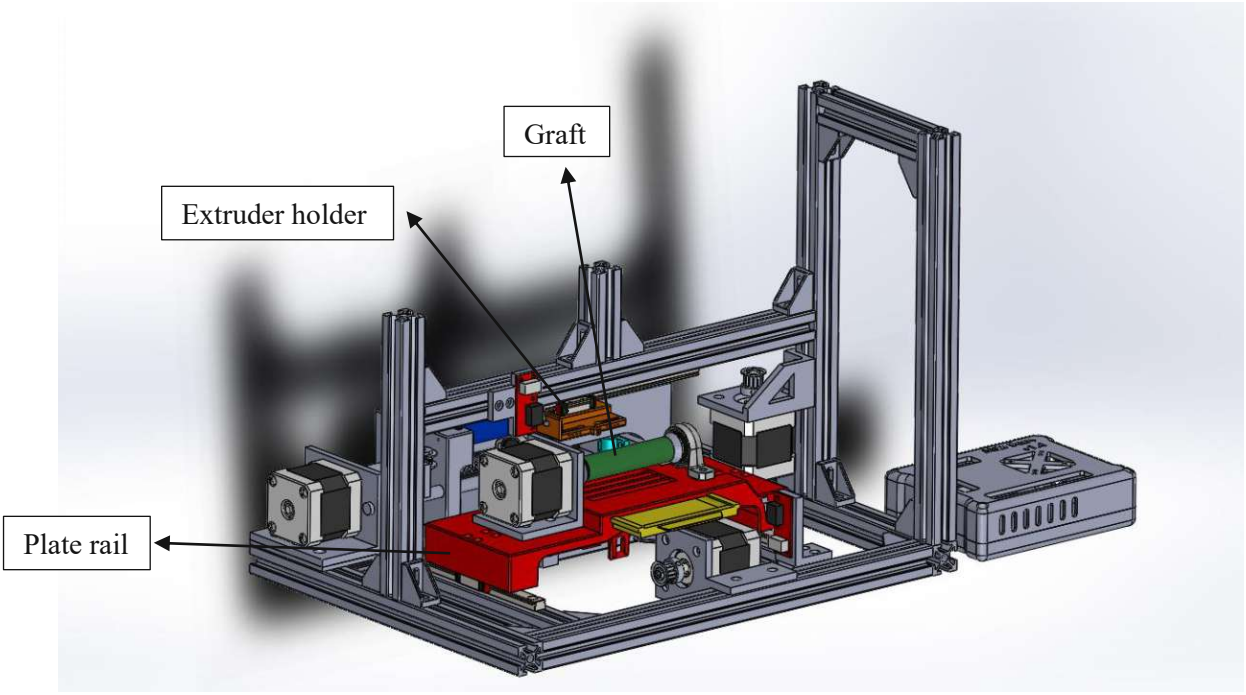

Figure 6: CAD design, front view

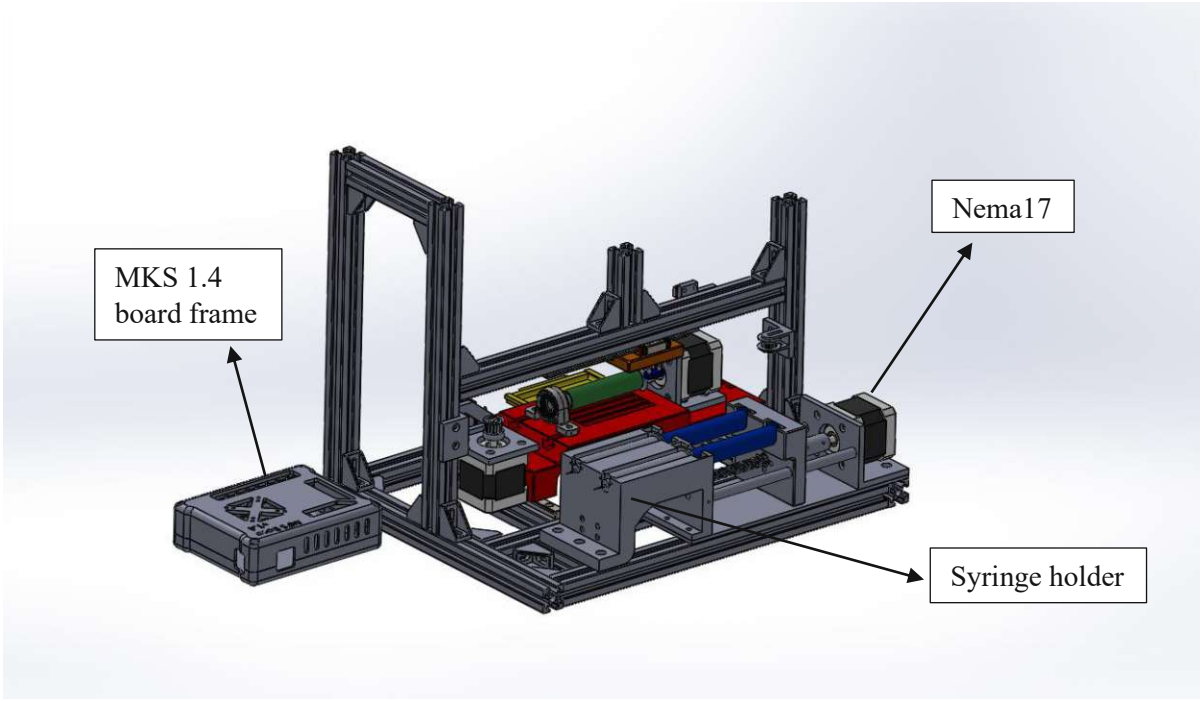

Figure 7: CAD design, back view

Some of the device components are built via 3D printing and other components (e.g. aluminum parts) are bought from a company (Metalland). The frame of the device is based on an aluminum profile 20, with a tensile strength of 250 N/mm², a density of 2.7 g/cm³, and an elastic module of 70,000 N/mm². In addition, brackets have been used to connect and fix the aluminum profiles together, which makes the cell seeding skeleton more stable and solid during seeding.

2.3. Syringe holder

Two syringe holders are implemented in our design, one for fibrinogen used as a cell carrier, and for thrombin. The advantage of using fibrin would be entrapping cells in the entangled protein fibrils. Thrombin is one of the blood-clotting enzymes involved in the coagulation cascade. It is produced from its inactive precursor, factor II prothrombin by enzymatic cleavage. Thrombin activates the blood coagulation factors V, VIII, XIII and initiates the final step in the coagulation cascade.

Figure 8 illustrates the cross-linking of fibrinogen via thrombin where a three-dimensional structure is created.

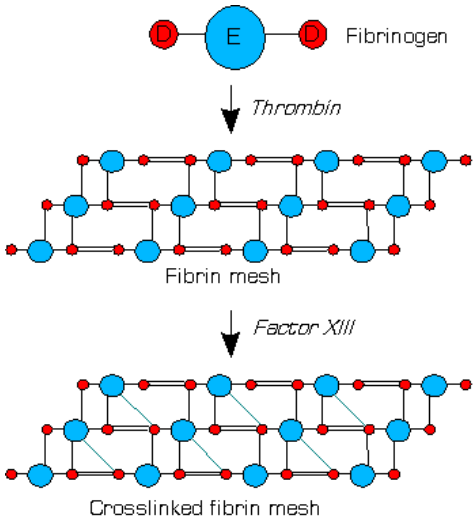

Figure 8: Cross-linking through thrombin (source: Wikipedia)

The extruder is fixed above the graft to allow fibrinogen and thrombin polymerization and simultaneous cell seeding right on site. To this end, a tubing system is implemented and used to connect the syringes to the extruder. The syringe holder allows for the manual adjustment of the syringe pistons to accommodate different seeding volumes.

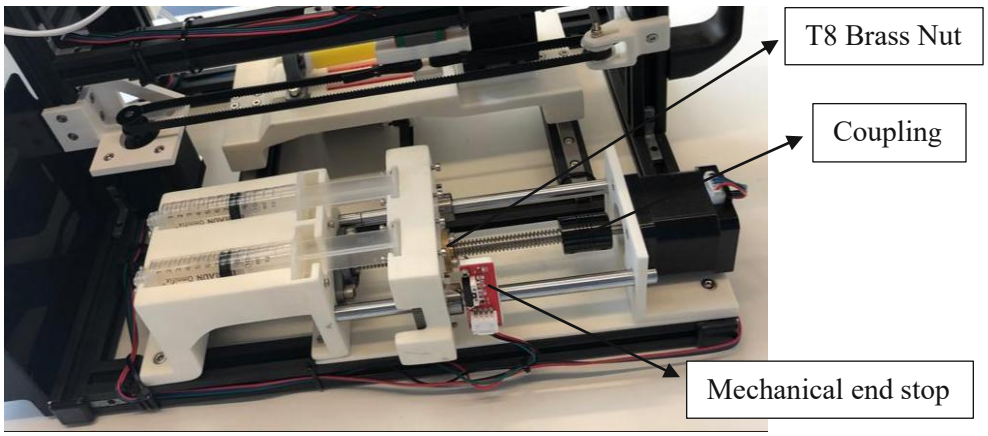

Figure 9: Syringe holder

As it can be seen in figure 9, a lead screw nut and nut holder are used. The lead screw nut has a good strength and wear resistance, hard to rust, high accuracy, and has good performance due to long usage spans and low friction coefficients. It can withstand great weight, is durable with high precision, and is easy to install. The material is a copper nut, stainless steel lead screw with 8 mm of diameter, 2 mm of spacing, and 2 mm of thread lead. The nut material is brass, and it has a diameter of 8 mm, a pitch of 2 mm, and a lead of 2 mm. The shaft coupling is made of aluminum with a length of 25 mm and a diameter of 18 mm. It is easy to use, durable, it does not rust and there is no need to process it. Beneath the syringe holder, a very small vibrator is fixed to prevent cells from settling (Figure 10). This vibrating motor (3V, 150 mA, 12 mm length and 6 mm diameter) is fixed beneath the syringe holder to provide a vibration to the syringes, which helps to heterogeneously distribute the cells for seeding. The vibration motor is user-friendly and powerful, with an operating range between 1.7 and 3.6 V DC, with revolutions: 10,000 +/- 2,500 rpm, starting voltage 0.7 V DC, starting current 200 mA, and insulation resistance of 10 MOhm.

Figure 10: Small vibrator, to prevent cells from settling

2.4. Extruder holder

The extruder component is able to move in the x-direction to seed the cells on the whole conduit surface. The speed varies from 1 mm/s up to 20 mm/s. The extruder design may vary depending on the needs. In fact, it is possible to seed the thrombin and fibrinogen separately, or they can be mixed just before exiting the tube.

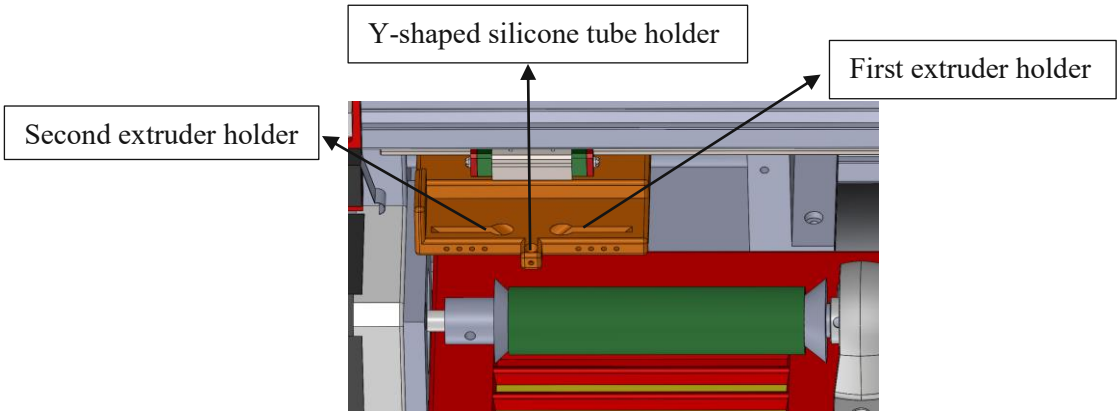

Figure 11: Extruder holder

As figure 11 illustrates, it is possible to fix one tube on the right and one on the left side of the tube holder. If needed, a needle (from 10 mm up to 25 mm in length) can also be connected to the head of the tubes and be fixed on the extruder

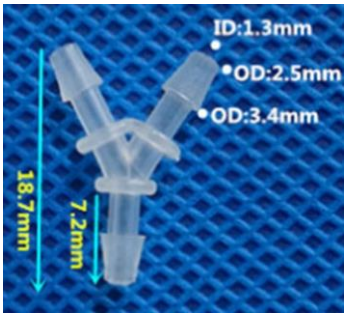

Figure 12: Y shaped silicone

Figure 12 illustrates a Y-shaped silicone tube, which can be fixed on top of the tube holder. The Y-tube allows for the simultaneous mixture of fibrinogen and thrombin which will then be seeded with cells on the graft. The design is based on the dimensions shown in figure 12, the diameter of the extruder in this Y-shaped silicone tube is 2.4 mm.

The extruder moves in the x-direction for 70 mm on top of the graft with different velocities by a pully and a GT2 (Gates Tooth) timing belt. The properties of the belt include the width of 6 mm, tooth height of 0.75 mm, belt height of 1.38 mm, working tension of 110 N for 25.4 mm belt width or 24 lbf for 1 inch, and breaking strength of 85 N Per 1 mm or 61 lbf per 1/8 inch belt width. The GT2 timing pulley is made from an aluminum alloy with 2 mm pitch and 16 teeth.

After each movement in the x-direction, the graft rotates by Nema17 and a bearing on the other side of the graft. Another strip line will be seeded after each rotation, and based on the angle of rotation, it is possible to have between 3 and 18 strip lines.

2.5. Graft holder

As it can be seen in figure 11, the bearing housing and coupling are necessary to fix the graft in its place below the extruder. The bearing housing is designed to support the conduit, it simplifies the shaft and bearing mounting, it protects the bearing from contaminant, and it extends the bearing operating life. Additionally, the bearing house helps to maximize functioning and provides customizable mounted bearing solutions, and it is cost-efficient. The coupling used as graft and syringe holder is a mechanical component that connects two shafts together, coupling and transmitting the power from the turning side to the turned side, while absorbing misalignment (mounting error) of the two shafts. Mounting errors, such as eccentricity or misalignment, inclined angle or core inclination, and axial direction displacement, are thereby avoided. The coupling shaft also absorbs vibration and shock to prevent damages and heat transfer to the motors and allow high precision movements.

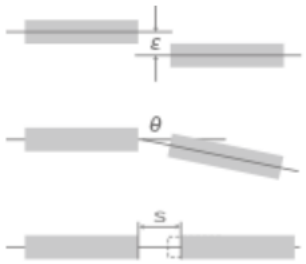

Figure 13: Mounting errors

Figure 13 illustrates different misalignments, including eccentricity, declination angle, and axial direction displacement between two shafts that can be absorbed by using a coupling.

A conical graft holder (Figure 14) is implemented in order to provide support to various graft diameters (up to 20 mm) and lengths. This holder provides a universal solution, and the conduit can be easily fixed in its final position.

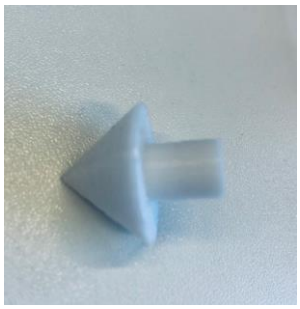

Figure 14: Graft holder

2.6. Plate rail

The plate rail is located beneath the graft and bearing, it moves in the y-direction (via a GT2 pulley and belt), while the graft rotates, and the extruder moves in the x-direction. Simultaneously the syringes start pumping fibrinogen, cells, and thrombin through the extruder to allow cell seeding. A movable plate inside the plate rail is designed to keep every component clean during the process. When the tube holder reaches the end of the conduit, the seeding is stopped, and the graft rotates. After rotation, the extruder starts to move in the opposite x-direction while seeding. These movements continue until the whole graft surface is seeded.

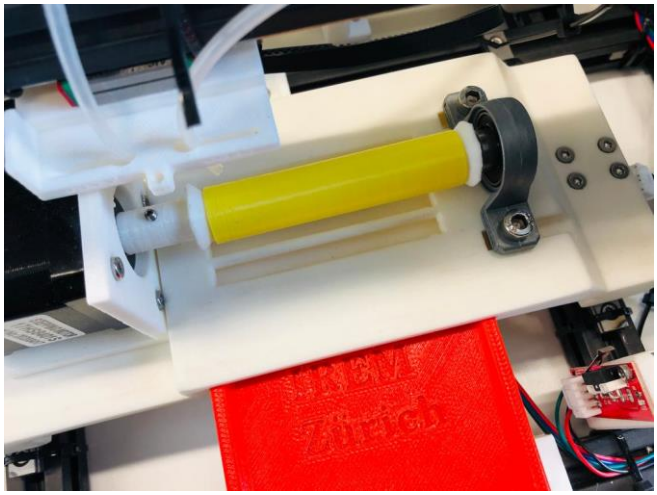

Figure 15: Plate rail, where graft, bearing and a motor are placed on it

2.7. 3D printing process

The syringe holder, plate rail and its plate, tube holder, graft holder, motor holder, and pulley holder, MKS frame, LCD display holder, and power holder are the components that are 3D printed due to the complex geometry and structure.

To prepare these components for the 3D printing company (3D Hubs), the CAD files are converted to a Standard Tessellation Language (STL) format. An STL file is a format that without any texture, colors, or other attributes defines the surface geometry of a 3D object.

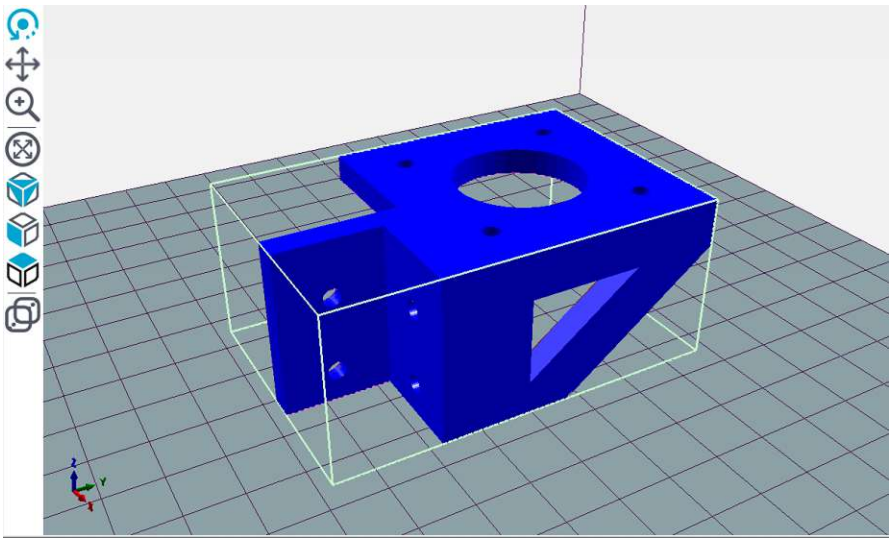

Figure 16: Motor holder, Repetier-Host

Figure 16 illustrates the motor holder in the x-direction. Repetier-Host is used as the 3D printing application.

There are different 3D printing processes available, including FDM, Selective Laser Sintering (SLS), Multi Jet Fusion (MJF), Stereolithography (SLA), and Direct Metal Laser Sintering (DMLS).

The FDM process is the most popular process in the 3D printing field. FDM printers extrude thermoplastic filament, layer by layer, which is heated to its melting point to produce a 3D object. The standards materials for FDM include Polylactides (PLA), Nylon, Polyethylene terephthalate (PET), Polyetherimides (PEI), Acrylonitrile-styrene-acrylate copolymers (ASA), and Thermoplastic Polyurethane (TPU). SLS is the ideal method to produce end-use parts by sintering polymer powder particles with a laser. MJF is used to manufacture precise and high-resolution objects with high surface quality and low porosity. It also produces functional plastic parts that can be used for end-use or detailed prototyping in small batches with isotropic mechanical properties. SLA belongs to the Vat Photopolymerization family and is the oldest patented process. In this process, light causes chemical oligomers and monomers to cross-link together to form a polymer. SLA is fast and can manufacture any design, however, it is an expensive process. DMLS is an industrial 3D printing process that manufactures fully functional metal prototypes with complex geometries. It melts and fuses layers and metallic powder with a high-power laser beam. Aluminum and stainless steel can be used as starting materials for this process.

Among the different additive manufacturing processes that have been mentioned FDM, SLS and MJF are suitable for the cell seeding device. In this project, 3D printing parts were manufactured by the FDM process due to its fast delivery and cost-efficiency. Standard PLA was considered as the material with 20% infill, and 100 µm layer height. The parts were manufactured with a dimensional accuracy of ± 5% with a lower limit of ± 0.5 mm and with a uniform surface texture without delamination or dents.

Figure 17 illustrates the completed cell seeding device. On the right side of the device, a graphic smart display controller is fixed, as well as a MKS 1.4 board and power supply.

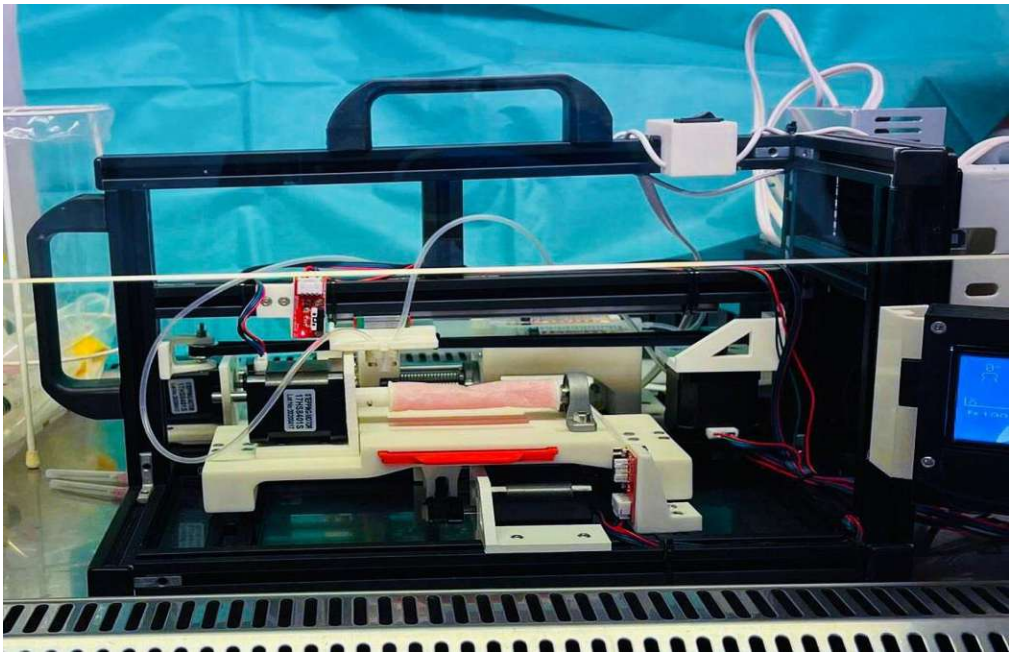

Figure 17: Automated cell seeding device

3. Cell seeding device electronics

3.1. Motherboard control board

As there is no specific Printed Circuit Board (PCB) for a cell seeding device, currently-available boards for 3D printers are used for this study. Usually, for custom 3D printers, an Arduino board with Ramps 1.4 shield that is positioned on the Arduino board pins (12 V power supply) are used. However, in this study, MKS 1.4 has been used as the motherboard. The clear advantage of the MKS board is that it improves and combines Arduino Mega 2560 with the Ramps 1.4 shield and provides a single feature-rich all-in-one electronics solution. In addition, MKS features onboard ATmega2560 and supports any power supply from 12V-24V. ATmega2560 is a high performance, low-power CMOS Microchip 8-bit based on the AVR enriched RICS architecture. RICS microcontroller combines 8KB SRAM, 86 general purpose I/O lines, 256 KB ISP flash memory, 4 KB EEPROM, 32 general purpose working registers, four USARTs, real-time counter, PWM, six flexible timer/counters with compare modes, byte-oriented Two-Wire serial interface, JTAG interface for on-chip debugging, and 16-channel 10-bit A/D converter. The device operates between 4.5-5.5 volts and when powerful instructions are executed in a single clock cycle, the ATmega2560 reaches throughput 16 MIPS at 16 MHz, allowing the system designer to balance both, the processing speed and the power consumption.

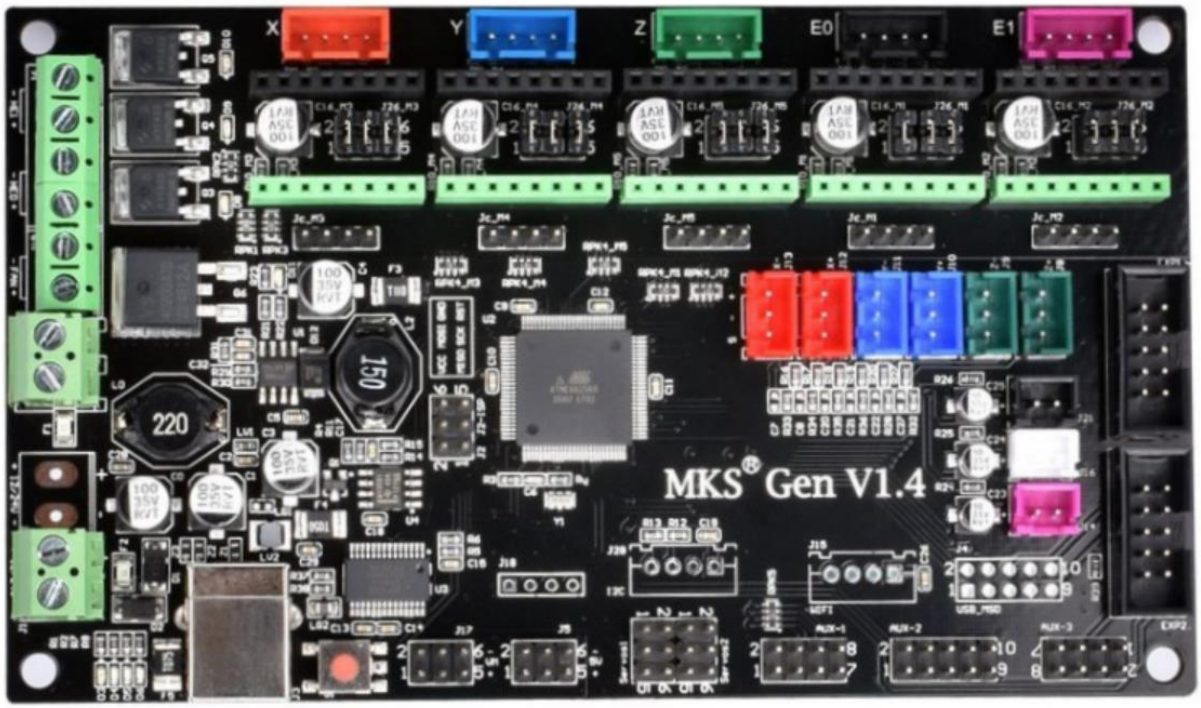

Figure 18: MKS Gen V1.4

Up to 5 stepper motors can be easily mounted on the motherboard. It also integrates Ramps 1.4 and maga2560, it supports replaceable DRV8825 and A4988 motor driver, 4 high-quality layer

PCB optimizes heat dissipation, the Ramps are designed with 2 shelves on top of each other, with better heat dissipation, it uses high-quality MOSFET tube, for thermistors, it has 3 temperature ADC connector, three 5V output, and three 12V-24V output interfaces. In addition, for short-circuit protection, it contains a recoverable fuse. Firmware and its configuration are the same as Ramps 1.4 and Marlin can be used as open-source firmware.

3.2. Connection of the stepper motors

As it is illustrated in figure 19, five stepper motors can be connected to the board. X, Y, and Z are the three stepper motors for the movement in individual axes, furthermore, E0 and E1 are the two extruders. In this study, we use E1 for the rotation of the graft, and Z for the syringes.

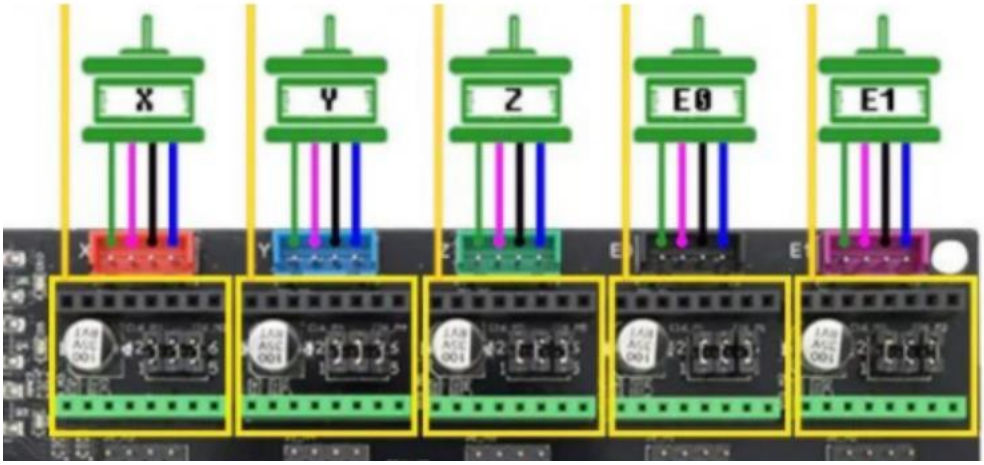

Figure 19: Connection of the stepper Motors

Nema17HS8401 have been used as the stepper motors. The stepper motors are electromagnetic brushless DC motors that transform digital pulses into mechanical shaft rotation and divide a full 360-degree circle into a number of equal steps. The Nema17 that has been used in this project has a step angle of 1.8 degree, which is equivalent to 200 steps per revolution. Micro-stepping is a method to run the stepper motor with more accuracy by sending a sine or cosine waveform to the coils to increase the number of steps. The advantage of using the stepper motor is that by its rotation via fractional increments it has a precise positional control. The dimension of the Nema17 is 42 x 42 x 47 mm (1.7 x 1.7 inch) with the holding torque of 550 mN mm and 20 mN m positioning torque, 5 mm of shank diameter, 22 mm of shaft length with 1.7 A/phase current consumption. The Nema17 model 17HS8401 is a two-phase stepper motor with DC 3V nominal voltage and 1.68 nominal current. The weight of the stepper motor Nema17 is 375 g, this is important to be considered for designing the motor holders.

As we do not want to damage the cells due to the heat dissipation by stepper motors it is important to consider the working temperature. Power is proportional to square of the current (P=I2R) and temperature rise is proportional to the power, however torque is directly proportional, consequently, it is possible without losing torque to keep the temperature under control. For instance, running the stepper motor at 70 percent of the rated current results (0.72=0.49) 49 percent of the thermal rise and power dissipation, and 70 percent of the torque. In the other words, with losing a little torque or motion we can lose a lot of heat as torque is proportional to current, and heat is proportional to current square. To avoid severely overheating the stepper motor, the device needs to work under its rated current amps, if the motor exceeds its rated current, the stepper motor will overheat and eventually die a quick death.

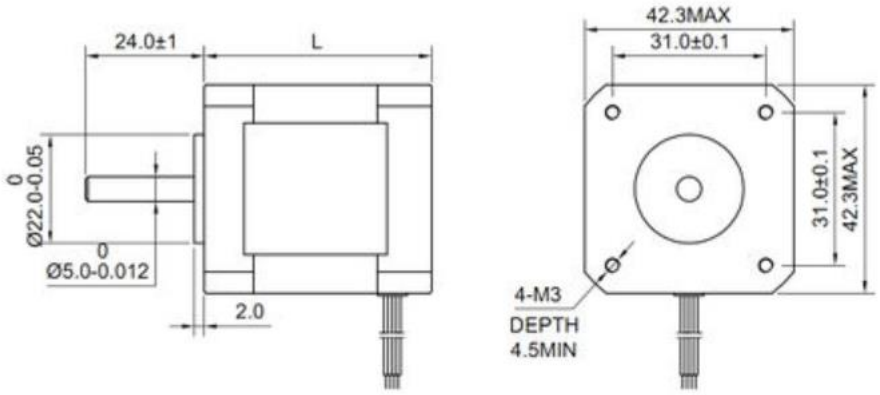

Figure 20: NEMA 17

To rotate the mechanical wheel one step at a time, the Nema17 (Figure 20) uses electromagnets and gear-like toothed. When a high pulse is sent, the coil is energized and it attracts the nearest teeth, subsequently, the motor performs one step. The speed of the motor is determined by the frequency of the pulse, the spinning direction of the stepper motor is determined by the sequence of the pulses, and with the number of pulses, it is possible to determine how far the motor rotates. Furthermore, at given rated current/torque the motor is rated for a 50 °C temperature rise. Stepper motors rated for 1-1.5 A and 3-5 V, generally perform near their peak torque with the current limiting controller. The main disadvantage of Nema17 is that with increasing speed the torque decreases, however, the advantages of it are high reliability, low cost, and possibility to operate in an open-loop control system. In addition, since Nema17 has an accuracy of 3-5% of a step and it is non-cumulative from one step to the other, it has precise positioning and movement reproducibility, which makes the Nema17 an outstanding choice for this study.

3.3. Stepper motor driver

A stepper motor driver is an electronic device that works as an interface between the control circuit and the motor. The controller is a device with low power output capability, and it cannot

produce enough current and voltage required by the stepper motor, consequently a driver is needed. The basic function of the stepper motor driver is to take a low current control signal and generate a higher one to move the motor axis. Since the stepper motor has a minimum of two coils, at least two H-bridges are needed to drive the motor.

The Pololu motor driver DRV8825 (figure 21) was chosen for this study, and it features a limiting amperage, undervoltage shutdown, over-temperature and over-current protection, and six micro-step resolutions (full, half, 1/4, 1/8, 1/16, and 1/32 step). It can deliver up to 1.5 A per phase, and with adequate cooling it is designed to control a bipolar stepper motor with an output current of up to 2.2 A. In addition, it operates between 8.2 V and 45 V which is ideal for the Nema17. M0, M1, and M2 are three step size or resolution, and the motors can be set to one of the six step resolutions shown in table 1. If these microstep pins are disconnected, the full-step mode will be activated, as all selector inputs contain 100kΩ internal resistors. If the current level is not set low enough, the micro-step modes will not function properly, the motor current does not get engaged, and subsequently, the micro-steps will be skipped by the motor. Jumpers are important components used to handle the resolution of the stepper motors.

STEP and DIR are the two control inputs of the DRV8825. Each pulse to the STEP input controls one micro-step of the motor, therefore the motor will rotate faster when the pulses are faster. The direction of the motor is selected by the DIR pin. The motor drives clockwise when it is driven HIGH, and it drives counterclockwise when it is driven LOW. When DIR is tied directly to GND or VCC, the motor rotates just in a single direction. RESET, SLEEP, and ENBL are three different inputs for controlling the DRV8825 power states. The driver became enabled when EN pin is driven LOW or logic 0. It is possible to connect any bipolar stepper motors from 8.2 V up to 45 V to the B2, B1, A1, and A2 output pins, each of them can deliver up to 2.2 A to the motor depending on current limitation setting, system's power supply, and cooling system.

MODE0	MODE1	MODE2	Microstep Resolution
Low	Low	Low	Full step
High	Low	Low	Half step
Low	High	Low	1/4 step
High	High	Low	1/8 step
Low	Low	High	1/16 step
High	Low	High	1/32 step
Low	High	High	1/32 step
High	High	High	1/32 step

Table 1: Microstep resolution

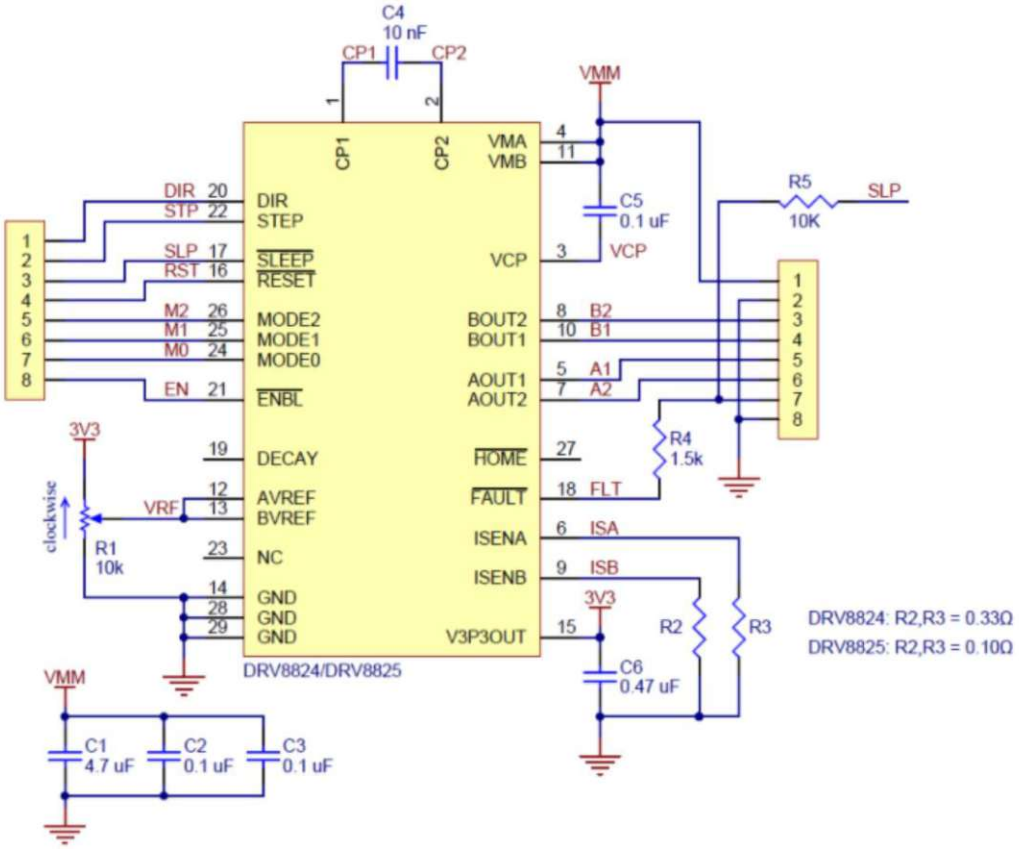

Figure 21: Schematic diagram DRV8825

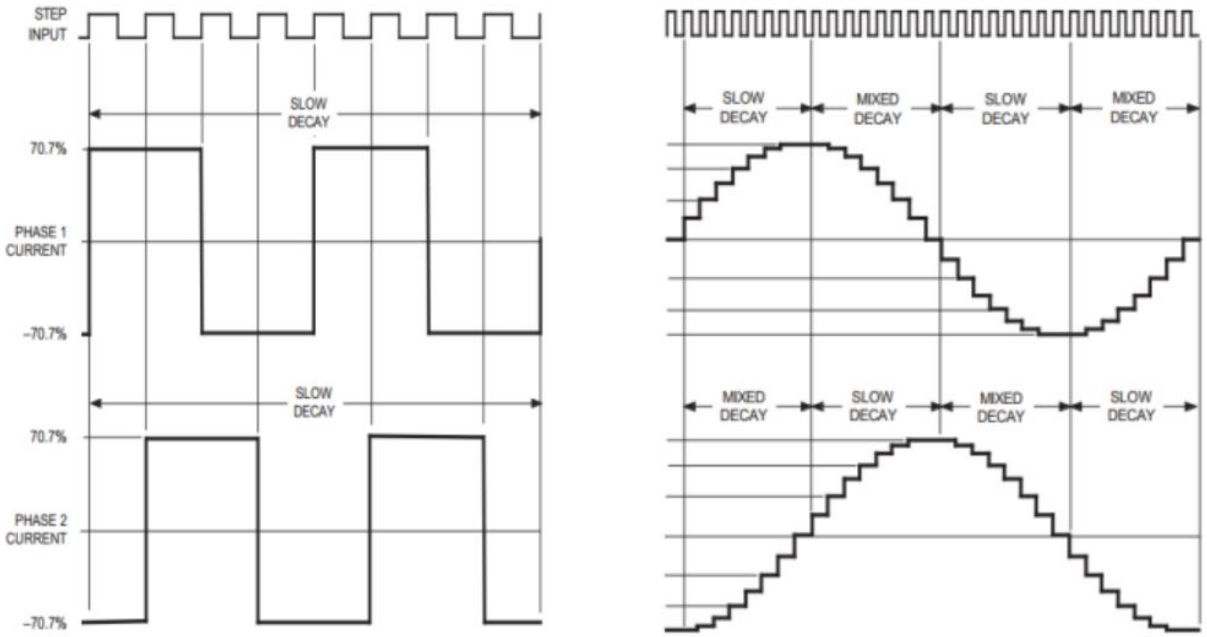

Figure 22: Full-step operation vs 8 microstep/step operation

Figure 21 illustrates the schematic diagram DRV8825, the diagram can be found in datasheet DRV8825 Stepper Motor Driver Carrier (https://www.pololu.com/product/2133). As it is shown in figure 22, by selecting a higher micro-steping value, the output changes and it becomes more like a sine wave, consequently, the motor will have smoother movements while producing enough torque.

3.4. Heatsink

However, the maximum current rating of the DRV8825 is 2.2 A per coil, the actual current that is possible to deliver depends on how well the IC is kept cool. It must be noted that when the chip supplies more than approximately 1.5A per coil it gets overheated, therefore, a heatsink is required to achieve more than 1.5A per coil. An aluminum heatsink will optimize the heat transfer between the surrounding environment and the chip when it is fixed with a thermal compound on the DRV8825 chip

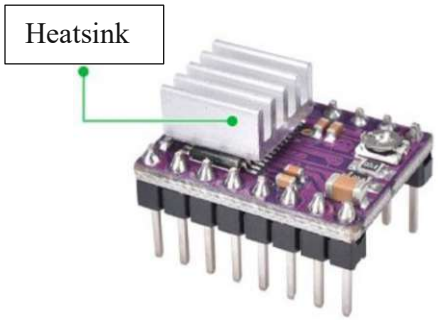

Figure 23: Cooling system

3.5. Limiting the current

Before using the motor, the stepper driver requires a slight adjustment. The maximum amount of current needs to be limited to ensure that it is not over- or underpowering the motor, in other words it is preferred to prevent exceeding the motor's rated current. To provide enough amount of torque, over- or underpowering is important to run without overheating. For example, with 5Ω coil resistance and a maximum current rating of 1A, reveals a maximum stepper motor supply of 5V, when this motor is used with 12V it permits higher step rates, however, to prevent damage to the stepper motor the current must be limited under 1A actively. On the DRV8825 driver, there is a small trimmer potentiometer that is used to set the current limit at or lower than the current rating of the stepper motor. There are two methods to make this adjustment:

3.5.1. First method

Here, the current is limited by measuring the voltage or Vref on the "ref" pin. Then, by leaving the three micro-step pins disconnected, the driver is put into full step and the motor is kept at a fixed position without clocking the STEP input. The voltage or Vref is measured while we adjust it on the metal trimmer pot. The Vref is adjusted by using the following formula:

Current limit = Vref × 2 → Vref = $I_{max}/2$

For example, for the motor rated 1.58A, Vref = 1.58/2 → Vref = 0.79

To not run the motor at the maximum rated current, a 10% safety margin needs to be implemented:

0.79 × 10/100 = 0.079 → Vref = 0.79 – 0.079 = 0.711V

A multi-meter is needed to work out what the current Vref is, 2V DC option must be selected as we are dealing with DC voltage. To have a correct reading, the board should be fully powered by the power supply. The red probe is used on the potentiometer and the black probe is used on the Ground pin. In our case the stepper motor is set to 1.3, By rotating the potentiometer clockwise, it is possible to decrease the Vref. As it is not easy to get the value spot on, setting the Vref slightly lower would be better than being set higher.

Figure 24: Measuring points

3.5.2. Second method

In the second method, the current limit is set by measuring it through the coils. Like the first method, after looking on the datasheet for the rated current of the stepper motor, the driver is set into full-step mode. The motor is held fixed by not clocking the STEP mode, the actual current flowing is measured while the ammeter is placed in series with one of the coils of the motor. Until the rated current is reached the current limited potentiometer will be adjusted by a small ceramic screwdriver. If ever the logic voltage or VDD changes, this adjustment needs to be repeated.

3.6. Mechanical end stop V1.2

Mechanical end stop limit switches used for the cell seeding device are the simplest and the most common adopted for 3D printers. They are contact-based manual switches that detect when an object has reached the end of its axis path. The mechanical end stop uses a single touch sensor. When the sensor is touched, it sends the signal to the board that the object is at the end of the path. In addition, it prevents the hardware from damage.

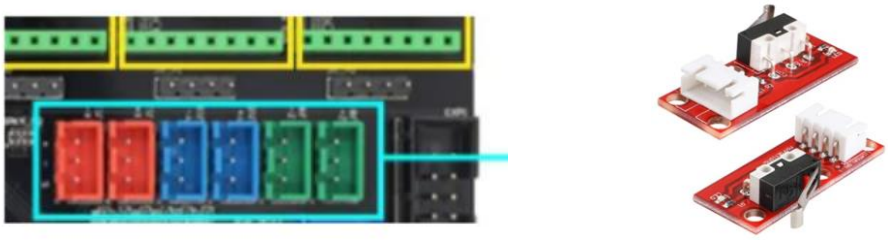

(A) **(B)**

Figure 25: (A) Connection of the end stop switch. **(B)** Mechanical end stop

On the MKS the pins for plugging the stepper motors are determined in different colors, the red one stands for the movement in the X-axis, blue stands for the movement in the Y-axis and the green stands for the Z-axis or for the syringes in this study. To make the connection, the green line connects to the signal, the black cable connects to GND and the red line connects VCC. The three end stops that are used in this study are positioned at the limits of the X, Y, and Z movement to find the zero coordinate of the X, Y, and Z-axis. The stepper motor is switched off when the object hits the end stop and sets the current coordinate of the end stop that has been activated to zero.

3.7. Graphic smart display

A full graphic smart display controller (Kingprint LCD 12864) has been used to control the seeding. It contains a rotary encoder that will be used for calibration and axes movement, a large screen 128 × 64 (3.2-inch) matrix display, and a SD card reader on the back, which supports 8 GB. To add support in the Marlin, the basic requirement is to define REPRAP_DISCOUNT_FULL_GRAPHIC_SMART_CONTROLLER in the "Configuration. h". EXP1 and EXP2 are the two fourteen pin pitch box connectors on the mainboard and display.

The two EXP1 and EXP2 are connected by a ribbon cable, which offer polarity-proof plugs that can be connected only in one direction.

Figure 26: Kingprint LCD 12864, graphic smart display controller

3.8. Power supply

High quality 12V 10A LEDMO switching power supply has been used in this study. The power supply transforms 110V to220 V Alternative Current (AC) found in a home to a Direct Current (DC) which is appropriate for the electronics and the components.

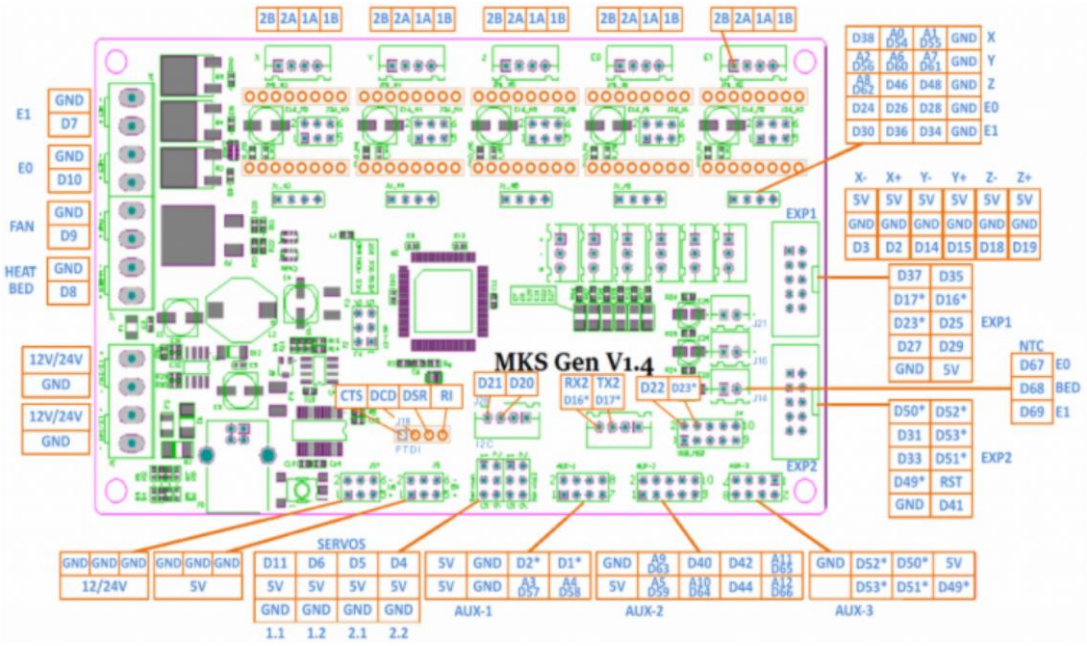

Figure 27: MKS Gen V1.4, all the details

4. Programs

To communicate between the hardware and software, a firmware is needed. When the software sends G-codes to the hardware of the cell seeding device, it automatically translates and interprets the G-codes into a specific form of electrical signals that are recognized by the motors and the other components of the device. Repetier Host has been used as the software and Marlin as the firmware in this study.

4.1. Firmware installation

As a first step, the Arduino IDE has to be downloaded (https://www.arduino.cc/en/software). As figure 28 illustrates, Arduino Mega 2560 is selected from the tools in Arduino IDE. Subsequently, also the 12864 LCD Marlin firmware is downloaded.

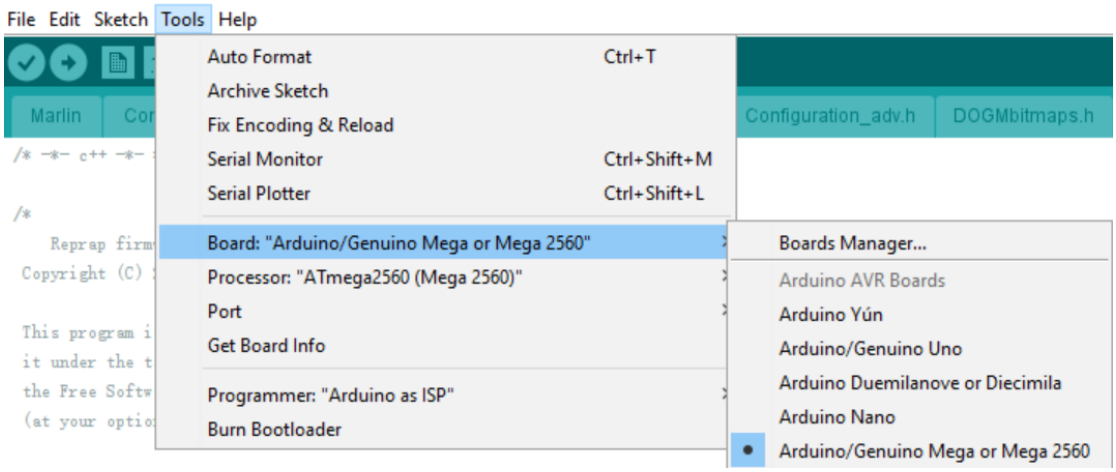

Figure 28: Firmware installation

After setting the changes for X, Y, and Z DIR, the firmware will be converted by the Arduino IDE into Mega2560 board. Since our device possess an additional DOF, which allows for graft rotation, the downloaded software is not able to automatically generate the necessary G-codes. Therefore all the G-codes have been specifically written for the seeding device (see paragraph 4.2). One sample of G-codes for 20 degree of rotation angle and 1mm/s velocity are reported in the appendix. In this sample the device seeds 18 strips line of the human dermal fibroblast cells directly onto the scaffold, while the velocity is 1mm/s.

4.2. G-codes

G-code is the most common programming language that has been used for computer numerical control (CNC) and it dictates the movement speed, the direction, and the path to the motor. 48 G-codes with different rotation angles of the graft and operation velocities have been written for this study (see appendix).

Rotation angle (degree)	Velocity (mm/s)							
20 degree	1mm/s	3mm/s	5mm/s	7mm/s	9mm/s	11mm/s	15mm/s	20mm/s
30 degree	1mm/s	3mm/s	5mm/s	7mm/s	9mm/s	11mm/s	15mm/s	20mm/s
45 degree	1mm/s	3mm/s	5mm/s	7mm/s	9mm/s	11mm/s	15mm/s	20mm/s
60 degree	1mm/s	3mm/s	5mm/s	7mm/s	9mm/s	11mm/s	15mm/s	20mm/s
90 degree	1mm/s	3mm/s	5mm/s	7mm/s	9mm/s	11mm/s	15mm/s	20mm/s
120 degree	1mm/s	3mm/s	5mm/s	7mm/s	9mm/s	11mm/s	15mm/s	20mm/s

Table 2: Rotation angles and velocities

As it can be seen in table 2, to find the best way of cell seeding, 8 different velocities have been considered for each angle to be tested in this study. For example, when the rotation angle is 120 degree, it divides the graft into three parts, consequently there will be three strip lines with 8 different velocities for axial movement. Eventually the device will be set to its initial place when the seeding is done. The dictionary of the codes can be found on https://reprap.org/wiki/G-code.

For instance, G00 is for rapid movement to a specific coordinate position, which is followed by a geometric location. For example, the code G0 X20 Y20 means moving to 20 mm on the X-axis, and 20 mm on the Y-axis, whereas G04 indicates the period of time which pauses the machine. On Marlin the "P" parameter will wait in milliseconds (ms) while the "S" will wait for seconds, therefore, G04 P2000 is equivalent to G04 S2. In this case the device will not move and will pause for 2000 ms. The state of the machine will be preserved and controlled during delays. G28 or move to the home (origin) is another important command that can be used without any additional parameters. For instance, when the firmware receives the G28 X Y Z command, it immediately moves all the specified axes to the end stop. If no axes are given, it moves all the axes to the endstops.

The other letters of the code have additional functions. The M-code, like the G-code, is a set for auxiliary commands, and is referred to the miscellaneous codes and functions. All the machine's

non-geometric actions, such as stopping programs, are controlled by the M commands. The variable A describes the absolute or incremental position of the A-axis, and it directs the tool around the X-axis. The definition of the positive rotation is a counterclockwise rotation looking from X positive towards negative.

As it can be seen in table 2, to find the most efficient cell seeding, 8 different operation velocities have been considered for each angle. For example, when the rotation angle is 120 degrees, it divides the graft into three parts, consequently, there will be three strip lines with 8 different operation velocities for axial movement. The device will be set to its initial place when the seeding is done.

5. Proof-of-concept results

5.1. Scaffold preparation

The TEVG was produced with non-woven PGA meshes (thickness 1.0 mm; specific gravity 70 mg/m^3; Cellon) coated with 1% poly-4-hydroxybutyrate (P4HB, MW 1x10^6 TEPHA Inc.) in tetrahydrofuran (Fluka, Sigma-Aldrich). The PGA/P4HB scaffold was sutured to a stainless-steel mandrel with 6 cm length and 1.6 cm diameter. The scaffolds were sterilized one day before cell seeding with a 30 min incubation in 70% ethanol followed by 30 min incubation in PBS supplemented with 10% penicillin-streptomycin (Sigma) and 1% antibiotic-antimycotic solution (Sigma).

5.2. Cell Expansion and seeding

After expansion in standard medium (Advanced DMEM (Gibco), supplemented with 10% fetal bovine serum (FBS, Gibco), 1% GlutaMax (Gibco), and 1% penicillin-streptomycin (Lonza)), neonatal human dermal fibroblasts (hDFBs, CellSystems Biotechnologie Vertrieb Gmbg) were seeded onto the TEVG scaffolds (1x10^6 cells/cm^3, n=2) using fibrin as a cell carrier. Fibrin and thrombin with cells were loaded into the device syringes, gradually injected in the tubing system, and homogeneously distributed on top the polymeric conduit. The solutions were injected through a 10 ml syringe in consecutive strips of 60 mm length, ejected at a velocity of 3 mm/s, and with a resting time between strips of 1 s. After overnight incubation at 37 °C under static conditions in standard medium, the TEVGs were fixed in 4% PFA and further analyzed via histological assessment.

5.3. Efficiency, uniformity and viability of automated cell seeding device

To evaluate the seeding efficiency and uniformity of the device on the TEVGs, each scaffold (n=2) was cut into five serial equal-sized rings (Figure 29) and qualitatively analyzed via histology.

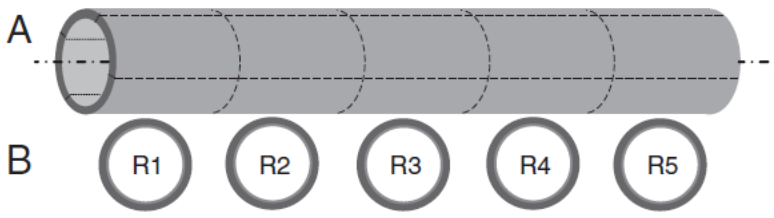

Figure 29: Schematic representation of the sample preparation procedure. The TEVG (A) is divided into five serial equal-sized rings (B).

5.4. Histological evaluation

After cutting the seeded scaffold into the rings, they were rinsed in PBS, and fixed in 4% PFA for 24 hours. Briefly, samples were then rinsed in PBS and dehydrated through graded ethanol washes and embedded in paraffin. The samples were cut with a slice thickness of 5 µm and stained with hematoxylin and eosin (H&E) to assess the tissue morphology and presence of cells. The stained samples were imaged with the brightfield microscopy (Mirax Midi Microscope, Carl Zeiss Gmhb) and viewed with the Pannoramic Viewer software.

5.5. Proof-of-concept results

The cell seeding has shown high uniformity along the longitudinal axis of the scaffold, and no significant differences in the number of cells was observed in the five consecutive scaffold rings. An overview of the histology staining of the TEVG is presented in Figure 30. The H&E staining shows a clear presence of cells on the surface and throughout the thickness of the TEVG, proving the efficacy of the device. Examination of the seeded cells at higher magnification (10X and 20X) showed that a large number of individual cells attached to the fibers of the scaffold and infiltrated through the polymeric scaffold.

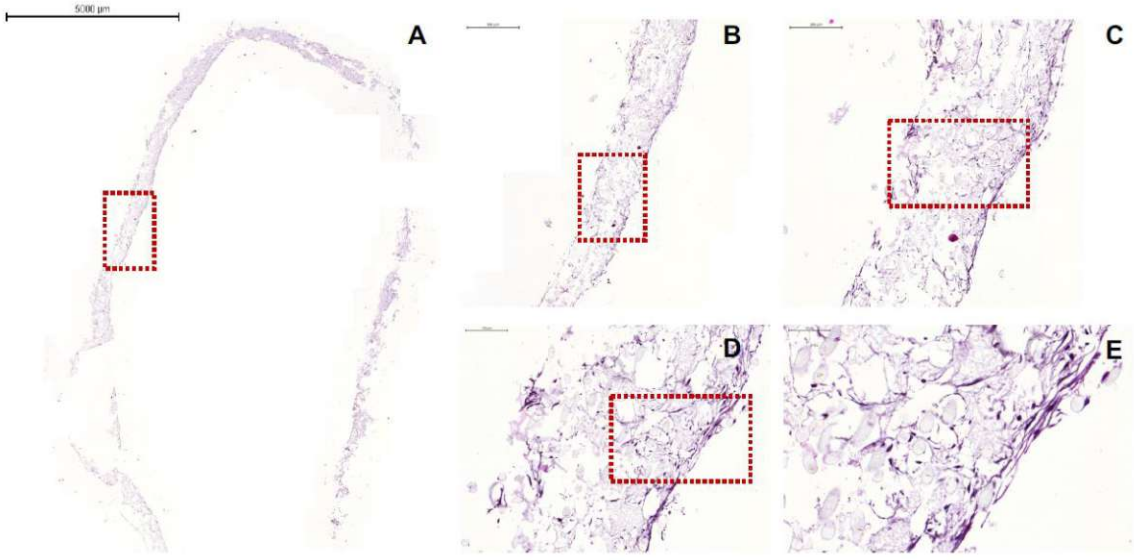

Figure 30: Histological evaluation of the seeding efficiency of the automated device. A) Full section of a TEVG ring stained with H&E (scale bar 5000 µm). B) 2X magnification picture of

the TEVG marked by the dotted rectangle in panel A (scale bar 500 μm). C) 5X magnification picture of the TEVG marked by the dotted rectangle in panel B (scale bar 200 μm). D) 10X magnification picture of the TEVG marked by the dotted rectangle in panel C (scale bar 100 μm). E) 20X magnification picture of the TEVG marked by the dotted rectangle in panel D (scale bar 50 μm). Cell nuclei are stained in blue, ECM and polymeric scaffold are stained in pink.

Application of post-rotation (4 rpm) to the seeded constructs for 30 min in an incubator significantly improved circumferential cell uniformity, without affecting the longitudinal uniformity.

5.6. Discussion

Cell seeding for vascular application on tubular structures (e.g. TEVGs) is a challenging and complex process, which homogeneity has to be granted to allow consistency and reproducibility. Manual cell seeding techniques have proven successful, in both the preclinical and clinical settings. However, they might introduce inter- and intra-operator variability, and therefore provide heterogeneous results and variability in the seeded grafts. This laborious step needs training, sufficient operator skills and, if working in a Good Manufacturing Practice (GMP) environment, a strict standard operating procedure guideline to ensure a homogeneous outcome. An automated cell seeding system, would therefore simplify the procedure, reduce time and costs, eliminate the risk of potential variability, and ensure reproducibility. Over the past years, several seeding methods have been developed, including centrifugal, rotational, electrostatic, and magnetic, that are capable of achieving significantly higher cell attachment to the scaffolds than manual seeding methods (76,85,91,104). However, also these methods present several drawbacks and are less user-friendly.

To evaluate the potential of automatization in the field of cardiovascular tissue engineering, we developed an operator-independent method for seeding hDFB on TEVGs. This study was designed to assess the seeding uniformity, efficiency, and reproducibility of a novel and automated seeding device that takes advantage of direct seeding of the cell, onto a rotating tubular scaffold.

To achieve uniform cell distribution along the graft and promote homogeneous tissue-like formation, the seeding process have to be controlled. Heterogeneous cells distributed within the scaffold result in the formation of naked areas and the migration of surrounding cells towards these areas, and late deposition of ECM, resulting in a spot-dependent tissue formation and potentially impaired functionality of the graft. Therefore, the seeding process must be carefully controlled to accomplish uniform cell distribution and promote homogenous tissue formation along the construct.

The method used in this study is a strip-based patterning seeding with the number of strips between 3 and 18 and distance (angle separation 120-20) can be changed by the G-codes

available on the screen. This technique permits the seeding of scaffolds with different diameters from 2 to 20 mm and lengths from 6 to 10 cm. Furthermore, the direct positioning of the cells in the longitudinal strips ensures a homogenous distribution along the total length of the scaffold of the cells. In this study, the automated seeding device was assessed on 60 mm length scaffolds with 4 strips (90 degrees angle separation) that were found to be optimal for seeding the construct. With this setup, long time periods of cell suspension are avoided, thereby improving cell viability. At the end of the seeding process, cell distribution demonstrated longitudinal uniformity. Immunostaining of the grafts confirmed the uniform distribution of the cells and the high-seeding efficiency in this method.

The seeding device reported in this study has been optimized for vascular tissue engineering applications, however, the device can potentially be extended to other tissue engineering fields (e.g. bone tissue engineering). Moreover, this seeding technique can be coupled to other methods to improve cell penetration in thick-walled scaffolds, for instance, the application of controlled vacuum. Additionally, this device would fasten the development of scaling-up technologies.

5.7. Limitations

This study has several limitations. First the number of samples used in this study was limited, but sufficient to prove the feasibility of the new approach. Second, the limited amount of time was sufficient to design and build the device, and provide a first proof-of-concept feasibility and functionality study with a relative analysis. Further in-depth analyses were out of the scope of this thesis, but will be addressed in the future.

6. Conclusion

To summarize, the optimal cell seeding technique requires a reliable method to increase the seeding efficiency, maximize homogeneous cell attachment, prevent excessive laboratory processing, and finally be time- and cost-effective. In this study, we designed and developed an automated cell seeding device for the direct deposition of vascular cells onto the tubular scaffolds. This technique avoids long periods of cells suspension as happens with rotational methods, and permits fast cell attachments to the grafts, this is particularly essential to prevent cell death. Furthermore, the direct deposition of cells onto the grafts reduces the detrimental effect on cell survival and cell morphology due to the high turbulence, high shear centrifugal methods. The automated cell seeding device in this study, allows optimal cell seeding on porous tubular scaffolds, the seeding in this method is done within minutes. Furthermore, the use of this automated cell seeding device provides a novel method for automated seeding of tubular scaffolds, moreover, it will avoid user-dependent errors and achieve controlled, homogeneous, and reproducible cell distribution on TEVGs, leading to a potential application in the GMP setting. Moreover, this seeding technique can be coupled to other methods to improve cell penetration in thick-walled scaffolds, for instance, the application of controlled vacuum. This study has several limitations, for instance, the number of samples used in this study was limited. However further in-depth analyses were out of the scope of this thesis but will be addressed in the future. Therefore, the weakness of this project would be the lack of quantitative evaluation to assess which parameters worked best and compare the tangible numbers to other seeding approaches.

6.1. Future work

Cell infiltration and device design can be further improved by coupling with other techniques. In particular, controlled vacuum model for thicker scaffolds could be applied. Furthermore, the software can be developed in a way that it automatically determines how many cells need to be seeded based on the geometry of different vessels. Finally, the device can be optimized and be combined with 3D bioprinting technologies.

7. Bibliography

1. Zoghbi W.A., Duncan T., Antman E., Barbosa M., Champagne B., Chen D., Gamra H., Harold J.G., Josephson S., Komajda M., Logstrup S., Mayosi B.M., Mwangi J., Ralston J., Sacco R.L., Sim K.H., Smith S.C., Jr, Vardas P.E., and Wood D.A. Sustainable development goals and the future of cardiovascular health: a statement from the global cardiovascular disease taskforce. *J Am Coll Cardiol* 64**,** 1385, 2014. DOI: 10.1016/j.jacc.2014.08.018

2. Mathers C.D., and Loncar D. Projections of global mortality and burden of disease from 2002 to 2030. *PLoS Med* 3**,** e442, 2006. DOI: 10.1371/journal.pmed.0030442

3. Van der Slegt J; Steunenberg SL; Donker JM The current position of precuffed expanded polytetrafluoroethylene bypass grafts in peripheral vascular surgery. *J. Vasc. Surg*. 2014, 60, 120–128. DOI: 10.1016/j.jvs.2014.01.062

4. Drews JD; Miyachi H; Shinoka T Tissue-engineered vascular grafts for congenital cardiac disease: Clinicalexperience and current status. *Trends Cardiovasc. Med*. 2017, 27, 521–531. DOI: 10.1016/j.tcm.2017.06.013

5. Langer R; Vacanti JP Tissue engineering. *Science* 1993,260, 920–926. DOI: 10.1126/science.8493529

6. Netter FH (2006) Atlas of human anatomy, 4th edn. Saunders, Philadelphia, PA

7. Johnston KW, Rutherford RB, Tilson MD, Shah DM, Hollier L, Stanley JC (March 1991). "Suggested standards for reporting on arterial aneurysms. Subcommittee on Reporting Standards for Arterial Aneurysms, Ad Hoc Committee on Reporting Standards, Society for Vascular Surgery and North American Chapter, International Society for Cardiovascular Surgery". *Journal of Vascular Surgery*. 13 (3): 452–8. DOI:10.1067/mva.1991.2673

8. Ma N, Wang SY, Sun YJ, Ren JH, Guo FJ. [Diagnostic value of contrast-enhanced ultrasound for accessory renal artery among patients suspected of renal artery stenosis]. Zhonghua Yi Xue Za Zhi. 2019 Mar 19;99(11):838-840. DOI: 10.3760/cma.j.issn.0376-2491.2019.11.008

9. Van Twist DJ, Houben AJ, de Haan MW, de Leeuw PW, Kroon AA. Pathophysiological differences between multifocal fibromuscular dysplasia and atherosclerotic renal artery stenosis. J Hypertens. 2017 Apr;35(4):845-852. DOI: 10.1097/HJH.0000000000001243

10. Dalen JE, Alpert JS, Goldberg RJ, Weinstein RS. The epidemic of the 20(th) century: coronary heart disease. Am J Med. 2014 Sep;127(9):807-12. DOI: 10.1016/j.amjmed.2014.04.015

11. European Stroke Organisation. Tendera M, Aboyans V, Bartelink ML, Baumgartner I, Clément D, Collet JP, Cremonesi A, De Carlo M, Erbel R, Fowkes FG, Heras M, Kownator S,

Minar E, Ostergren J, Poldermans D, Riambau V, Roffi M, Röther J, Sievert H, van Sambeek M, Zeller T., ESC Committee for Practice Guidelines. ESC Guidelines on the diagnosis and treatment of peripheral artery diseases: Document covering atherosclerotic disease of extracranial carotid and vertebral, mesenteric, renal, upper and lower extremity arteries: the Task Force on the Diagnosis and Treatment of Peripheral Artery Diseases of the European Society of Cardiology (ESC). Eur Heart J. 2011 Nov;32(22):2851-906. DOI: 10.1093/eurheartj/ehr211

12. De Paulis R; Scaffa R; A third generation of ascending aorta Dacron graft: preliminary experience. DOI: 10.1016/j.athoracsur.2007.05.073

13. Spadaccio C, Rainer A, Barbato R, et al. The fate of large-diameter Dacron (R) vascular grafts in surgical practice: are we really satisfied? *International Journal of Cardiology.* 2013;168(5):5028–5029. DOI: 10.1016/j.ijcard.2013.07.165

14. Chlupac, J., Filova, E., & Bacakova, L. (2009). Blood vessel replacement: 50 years of development and tissue engineering paradigms in vascular surgery. *Physiol Res, 58*(Suppl 2), S119–139. DOI: 10.33549/physiolres.931918

15. Bical OM, Heran J, Thebault B, et al. Pseudoaneurysm following Dacron replacement of the ascending aorta. *European Journal of Cardio-Thoracic Surgery.* 2009;35(3):536. DOI: 10.1016/j.ejcts.2008.12.013.

16.Tai NR, Salacinski HJ, Edwards A, et al. Compliance properties of conduits used in vascular reconstruction. *British Journal of Surgery.* 2000;87(11):1516–1524. DOI: 10.1046/j.1365-2168.2000.01566.x

17. Moreno MJ, Ajji A, Mohebbi-Kalhori D, et al. Development of a compliant and cytocompatible micro-fibrous polyethylene terephthalate vascular scaffold. *Journal of Biomedical Materials Research. Part B, Applied Biomaterials.* 2011;97(2):201–214. DOI: 10.1002/jbm.b.31774.

18. Ballyk PD, Walsh C, Butany J, et al. Compliance mismatch may promote graft-artery intimal hyperplasia by altering suture-line stresses. *Journal of Biomechanics.* 1998;31(3):229–237. DOI: 10.1016/S0197-3975(97)00111-5

19. Kim HB, Choi YH, So YH, et al. Tissue responses to endovascular stent grafts for saccular abdominal aortic aneurysms in a canine model. *Journal of Korean Medical Science.* 2012;27(10):1170–1176. DOI: 10.3346/jkms.2012.27.10.1170.

20. Masden D.L., Seruya M., and Higgins J.P. A systematic review of the outcomes of distal upper extremity bypass surgery with arterial and venous conduits. *J Hand Surg* 37**,** 2362, 2012 DOI: 10.1016/j.jhsa.2012.07.028

21. Athanasiou T., Saso S., Rao C., Vecht J., Grapsa J., Dunning J., Lemma M., and Casula R. Radial artery versus saphenous vein conduits for coronary artery bypass surgery: forty years of competition—which conduit offers better patency? A systematic review and meta-analysis. *Eur J Cardiothorac Surg* 40**,** 208, 2011 DOI: 10.1016/j.ejcts.2010.11.012

22. Cho K.R., Kim J.-S., Jae-Sung C., and Kim K.-B. Serial angiographic follow-up of grafts one year and five years after coronary artery bypass surgery. *Eur J Cardiothorac Surg* 29**,** 511, 2006 DOI: 10.1016/j.ejcts.2005.12.026

23. Goldman S., Zadina K., Moritz T., Ovitt T., Sethi G., Copeland J.G., Thottapurathu L., Krasnicka B., Ellis N., Anderson R.J., and Henderson W. Long-term patency of saphenous vein and left internal mammary artery grafts after coronary artery bypass surgery results from a Department of Veterans Affairs Cooperative Study. *J Am Coll Cardiol* 44**,** 2149, 2004 DOI: 10.1016/j.jacc.2004.08.064

24. Harskamp R.E., Lopes R.D., Baisden C.E., de Winter R.J., and Alexander J.H. Saphenous vein graft failure after coronary artery bypass surgery: pathophysiology, management, and future directions. *Ann Surg* 257**,** 824, 2013 DOI: 10.1097/SLA.0b013e318288c38d

25. Klinkert P., Post P.N., Breslau P.J., and van Bockel J.H. Saphenous vein versus PTFE for above-knee femoropopliteal bypass. A Review of the literature. *Eur J Vasc Endovasc Surg* 27**,** 357, 2004 DOI: 10.1016/j.ejvs.2003.12.027

26. Conte M.S. Critical appraisal of surgical revascularization for critical limb ischemia. *J Vasc Surg* 57**,** 8S, 2013 DOI: 10.1016/j.jvs.2012.05.114

27. Chew D.K.W., Owens C.D., Belkin M., Donaldson M.C., Whittemore A.D., Mannick J.A., and Conte M.S. Bypass in the absence of ipsilateral greater saphenous vein: safety and superiority of the contralateral greater saphenous vein. *J Vasc Surg* 35**,** 1085, 2002 DOI: 10.1067/mva.2002.124628

28. Taylor L.M., Jr, Edwards J.M., Brant B., Phinney E.S., and Porter J.M. Autogenous reversed vein bypass for lower extremity ischemia in patients with absent or inadequate greater saphenous vein. *Am J Surg* 153**,** 505, 1987 DOI: 10.1016/0002-9610(87)90803-8

29. Spadaccio C, Chello M, Trombetta M, et al. Drug releasing systems in cardiovascular tissue engineering. *Journal of Cellular and Molecular Medicine.* 2009;13(3):422–439. DOI: 10.1111/j.1582-4934.2008.00532.x

30. Baguneid M.S., Seifalian A.M., Salacinski H.J., Murray D., Hamilton G., and Walker M.G. Tissue engineering of blood vessels. *Br J Surg* 93**,** 282, 2006. DOI: 10.1002/bjs.5256

31. Sarkar S., Salacinski H.J., Hamilton G., and Seifalian A.M. The mechanical properties of infrainguinal vascular bypass grafts: their role in influencing patency. *Eur J Vasc Endovasc Surg* 31**,** 627, 2006. DOI: 10.1016/j.ejvs.2006.01.006

32. Haruguchi H., and Teraoka S. Intimal hyperplasia and hemodynamic factors in arterial bypass and arteriovenous grafts: a review. *J Artif Organs* 6**,** 227, 2003. DOI: 10.1007/s10047-003-0232-x

33. Owida A.A., Do H., and Morsi Y.S. Numerical analysis of coronary artery bypass grafts: an over view. *Comput Methods Programs Biomed* 108**,** 689, 2012. DOI: 10.1016/j.cmpb.2011.12.005

34. Scharn D.M., Daamen W.F., van Kuppevelt T.H., and van der Vliet J.A. Biological mechanisms influencing prosthetic bypass graft patency: possible targets for modern graft design. *Eur J Vasc Endovasc Surg* 43**,** 66, 2012. DOI: 10.1016/j.ejvs.2011.09.009

35. John L.C.H. Biomechanics of coronary artery and bypass graft disease: potential new approaches. *Ann Thorac Surg* 87**,** 331, 2009. DOI: 10.1016/j.athoracsur.2008.07.023

36. Rosso F; Marino G; Giordano A; Barbarisi M; Parmeggiani D; Barbarisi A Smart materials as scaffolds for tissue engineering. *J. Cell. Physiol*. 2005, 203, 465–470. DOI: 10.1002/jcp.20270

37. Engelmayr GC Jr, Sales VL, Mayer JE Jr et al (2006) Cyclic flexure and laminar flow synergistically accelerate mesenchymal stem cell-mediated engineered tissue formation: implications for engineered heart valve tissues. Biomaterials 27:6083–6095. DOI: 10.1016/j.biomaterials.2006.07.045

38. Mol A, Driessen NJB, Rutten MCM et al (2005) Tissue engineering of human heart valve leaflets: a novel bioreactor for a strain-based conditioning approach. Ann Biomed Eng 33:1778–1788. DOI: 10.1007/s10439-005-8025-4

39. Syedain ZH, Tranquillo RT (2009) Controlled cyclic stretch bioreactor for tissue-engineered heart valves. Biomaterials 30:4078–4084. DOI: 10.1016/j.biomaterials.2009.04.027

40. Williams C, Johnson SL, Robinson PS (2006) Cell sourcing and culture conditions for fibrin-based valve constructs. Tissue Eng 12:1489–1502. DOI: 10.1089/ten.2006.12.1489

41. Mol, A., Smits, A. I. P. M., Bouten, C. V. C. & Baaijens, F. P. T. Tissue engineering of heart valves: advances and current challenges. *Expert. Rev. Med. Devices.* 6, 259–275, 2009 DOI: 10.1586/erd.09.12

42. Bouten, C. V. C. et al. Substrates for cardiovascular tissue engineering. *Adv. Drug. Deliv. Rev.* 63, 221–241, 2011. DOI: 10.1016/j.addr.2011.01.007

43. Crapo PM; Gilbert TW; Badylak SF An overview of tissue and whole organ decellularization processes. *Biomaterials* 2011, 32, 3233–3243. DOI: 10.1016/j.biomaterials.2011.01.057

44. J. F. Mano, G. A. Silva, H. S. Azevedo et al., "Natural origin biodegradable systems in tissue engineering and regenerative medicine: present status and some moving trends," *Journal of the Royal Society Interface*, vol. 4, no. 17, pp. 999–1030, 2007. DOI: 10.1098/rsif.2007.0220

45. Couet F, Rajan N, and Mantovani D, "Macromolecular biomaterials for scaffold-based vascular tissue engineering," *Macromolecular Bioscience*, vol. 7, no. 5, pp. 701–718, 2007. DOI: 10.1002/mabi.200700002

46. Pankajakshan D, and Agrawal D.K, "Scaffolds in tissue engineering of blood vessels," *Canadian Journal of Physiology and Pharmacology*, vol. 88, no. 9, pp. 855–873, 2010. DOI: 10.1139/y10-073

47. Flanagan TC, Cornelissen C, The in vitro development of autologous fibrin-based tissue-engineered heart valves through optimised dynamic conditioning.
DOI: 10.1016/j.biomaterials.2007.04.012

48. Robinson PS, Jonson SL, Functional tissue-engineered valves from cell-remodeled fibrin with commissural alignment of cell-produced collagen. DOI: 10.1089/ten.a.2007.0148

49. B. Marelli, M. Achilli, A. Alessandrino et al., "Collagen-reinforced electrospun silk fibroin tubular construct as small calibre vascular graft," *Macromolecular Bioscience*, vol. 12, no. 11, pp. 1566–1574, 2012. DOI: 10.1002/mabi.201200195

50. S. G. Wise, M. J. Byrom, A. Waterhouse, P. G. Bannon, M. K. C. Ng, and A. S. Weiss, "A multilayered synthetic human elastin/polycaprolactone hybrid vascular graft with tailored mechanical properties," *Acta Biomaterialia*, vol. 7, no. 1, pp. 295–303, 2011.
DOI: 10.1016/j.actbio.2010.07.022

51. K. A. McKenna, M. T. Hinds, R. C. Sarao et al., "Mechanical property characterization of electrospun recombinant human tropoelastin for vascular graft biomaterials," *Acta Biomaterialia*, vol. 8, no. 1, pp. 225–233, 2012. DOI: 10.1016/j.actbio.2011.08.001

52. B. Zavan, V. Vindigni, S. Lepidi et al., "Neoarteries grown in vivo using a tissue-engineered hyaluronan-based scaffold," *FASEB Journal*, vol. 22, no. 8, pp. 2853–2861, 2008.
DOI: 10.1096/fj.08-107284

53. Grover, C. N. , Gwynne, J. H. , Pugh, N. , Hamaia, S. , Farndale, R. W. , Best, S. M. , and Cameron, R. E. , 2012, " Crosslinking and Composition Influence the Surface Properties, Mechanical Stiffness and Cell Reactivity of Collagen-Based Films," *Acta Biomater.*, 8(8), pp. 3080–3090. DOI: 10.1016/j.actbio.2012.05.006

54. Rose, J. , Pacelli, S. , Haj, A. , Dua, H. , Hopkinson, A. , White, L. , and Rose, F. , 2014, " Gelatin-Based Materials in Ocular Tissue Engineering," *Materials*, 7(4), pp. 3106–3135.
DOI: 10.3390/ma7043106

55. Sell, S. A. , Wolfe, P. S. , Garg, K. , McCool, J. M. , Rodriguez, I. A. , and Bowlin, G. L. , 2010, " The Use of Natural Polymers in Tissue Engineering: A Focus on Electrospun Extracellular Matrix Analogues," *Polymers*, 2(4), pp. 522–553. DOI: 10.3390/polym2040522

56. Lovett M., Eng G., Kluge J., Cannizzaro C., Vunjak-Novakovic G., and Kaplan D.L. Tubular silk scaffolds for small diameter vascular grafts. *Organogenesis* 6**,** 217, 2010.
DOI: 10.4161/org.6.4.13407

57. Pektok E; Nottelet B; Tille JC; Gurny R; Kalangos A; Moeller M Degradation and healing characteristics of small-diameter poly(ε-capro-lactone) vascular grafts in the rat systemic arterial circulation. *Circulation* 2008, 118, 2563–2570. DOI: 10.1161/CIRCULATIONAHA.108.795732

58. A. V. Piterina, A. J. Cloonan, C. L. Meaney et al., "ECM-based materials in cardiovascular applications: inherent healing potential and augmentation of native regenerative

processes," *International Journal of Molecular Sciences*, vol. 10, no. 10, pp. 4375–4417, 2009. DOI: 10.3390/ijms10104375

59. J. J. Song and H. C. Ott, "Organ engineering based on decellularized matrix scaffolds," *Trends in Molecular Medicine*, vol. 17, no. 8, pp. 424–432, 2011. DOI: 10.1016/j.molmed.2011.03.005

60. S. F. Badylak, D. O. Freytes, and T. W. Gilbert, "Extracellular matrix as a biological scaffold material: structure and function," *Acta Biomaterialia*, vol. 5, no. 1, pp. 1–13, 2009. DOI: 10.1016/j.actbio.2008.09.013

61. A. F. Pellegata, M. A. Asnaghi, I. Stefani et al., "Detergent-enzymatic decellularization of swine blood vessels: insight on mechanical properties for vascular tissue engineering," *BioMed Research International*, vol. 2013, Article ID 918753, 8 pages, 2013. DOI: 10.1155/2013/918753

62. Keane T.J., Londono R., Turner N.J., and Badylak S.F. Consequences of ineffective decellularization of biologic scaffolds on the host response. *Biomaterials* 33**,** 1771, 2012. DOI: 10.1016/j.biomaterials.2011.10.054

63. Spark J.I., Yeluri S., Derham C., Wong Y.T., and Leitch D. Incomplete cellular depopulation may explain the high failure rate of bovine ureteric grafts. *Br J Surg* 95**,** 582, 2008. DOI: 10.1002/bjs.6052

64. Roy S., Silacci P., and Stergiopulos N. Biomechanical proprieties of decellularized porcine common carotid arteries. *Am J Physiol Heart Circ Physiol* 289**,** H1567, 2005. DOI: 10.1152/ajpheart.00564.2004

65. Simon P., Kasimir M.T., Seebacher G., Weigel G., Ullrich R., Salzer-Muhar U., Rieder E., and Wolner E. Early failure of the tissue engineered porcine heart valve SYNERGRAFT® in pediatric patients. *Eur J Cardiothorac Surg* 23**,** 1002, 2003. DOI: 10.1016/s1010-7940(03)00094-0

66. Peck M., Gebhart D., Dusserre N., McAllister T.N., and L'Heureux N. The evolution of vascular tissue engineering and current state of the art. *Cells Tissues Organs* 195**,** 144, 2012. DOI: 10.1159/000331406

67. Kelm J.M., Lorber V., Snedeker J.G., Schmidt D., Broggini-Tenzer A., Weisstanner M., Odermatt B., Mol A., Zünd G., and Hoerstrup S.P. A novel concept for scaffold-free vessel tissue engineering: self-assembly of microtissue building blocks. *J Biotechnol* 148**,** 46, 2010. DOI: 10.1016/j.jbiotec.2010.03.002

68. Norotte C., Marga F.S., Niklason L.E., and Forgacs G. Scaffold-free vascular tissue engineering using bioprinting. *Biomaterials* 30**,** 5910, 2009. DOI: 10.1016/j.biomaterials.2009.06.034

69. Hoerstrup SP, Sodian R, Daebritz S et al (2000) Functional living trileaflet heart valves grown in vitro. Circulation 102:III44–III49. DOI: 10.1161/01.cir.102.suppl_3.iii-44

70. Mol A, Rutten MC, Driessen NJ et al (2006) Autologous human tissue-engineered heart valves: prospects for systemic application. Circulation 114:I152–I158. DOI: 10.1161/CIRCULATIONAHA.105.001123

71. Wang Z; Cui Y; Wang J; Yang X; Wu Y; Wang K; Gao X; Li D; Li Y; Zheng XL; Kong D; Zhao Q The effect of thick fibers and large pores of electrospun poly (epsilon-caprolactone) vascular grafts on macrophage polarization and arterial regeneration. *Biomaterials* 2014, 35, 5700–5710. DOI: 10.1016/j.biomaterials.2014.03.078

72. Janairo RRR; Zhu Y; Chen T; Li S Mucin covalently bonded to microfibers improves the patency of vascular grafts. *Tissue Eng. Part A* 2014, 20, e285–e293. DOI: 10.1089/ten.TEA.2013.0060

73. Shin'oka T. Matsumura G. Hibino N. Naito Y. Watanabe M. Konuma T. Sakamoto T. Nagatsu M. Kurosawa H. Midterm clinical result of tissue-engineered vascular autografts seeded with autologous bone marrow cells. J Thorac Cardiovasc Surg. 2005;129:1330. DOI: 10.1016/j.jtcvs.2004.12.047

74. L'Heureux N. McAllister T.N. de la Fuente L.M. Tissue-engineered blood vessel for adult arterial revascularization. N Engl J Med. 2007;357:1451. DOI: 10.1056/NEJMc071536

75. Niklason L.E. Gao J. Abbott W.M. Hirschi K.K. Houser S. Marini R. Langer R. Functional arteries grown in vitro. Science. 1999;284:489. DOI: 10.1126/science.284.5413.489

76. Roh J.D. Nelson G.N. Brennan M.P. Mirensky T.L. Yi T. Hazlett T.F. Tellides G. Sinusas A.J. Pober J.S. Saltzman W.M. Kyriakides T.R. Breuer C.K. Small-diameter biodegradable scaffolds for functional vascular tissue engineering in the mouse model. Biomaterials. 2008;29:1454. DOI: 10.1016/j.biomaterials.2007.11.041

77. Pawlowski K.J. Rittgers S.E. Schmidt S.P. Bowlin G.L. Endothelial cell seeding of polymeric vascular grafts. Front Biosci. 2004;9:1412. DOI: 10.2741/1302

78. Nasseri B.A. Pomerantseva I. Kaazempur-Mofrad M.R. Sutherland F.W. Perry T. Ochoa E., et al. Dynamic rotational seeding and cell culture system for vascular tube formation. Tissue Eng. 2003;9:291. DOI: 10.1089/107632703764664756

79. Yow K.H. Ingram J. Korossis S.A. Ingham E. Homer-Vanniasinkam S. Tissue engineering of vascular conduits. Br J Surg. 2006;93:652. DOI: 10.1002/bjs.5343

80. Parikh S.A. Edelman E.R. Endothelial cell delivery for cardiovascular therapy. Adv Drug Deliv Rev. 2000;42:139. DOI: 10.1016/s0169-409x(00)00058-2

81. Roh J.D. Nelson G.N. Udelsman B.V. Brennan M.P. Lockhart B. Fong P.M. Lopez-Soler R.I. Saltzman W.M. Breuer C.K. Centrifugal seeding increases seeding efficiency and cellular distribution of bone marrow stromal cells in porous biodegradable scaffolds. Tissue Eng. 2007;13:2743. DOI: 10.1089/ten.2007.0171

82. Mo X.M. Xu C.Y. Kotaki M. Ramakrishna S. Electrospun P(LLA-CL) nanofiber: a biomimetic extracellular matrix for smooth muscle cell and endothelial cell proliferation. Biomaterials. 2004;25:1883. DOI: 10.1016/j.biomaterials.2003.08.042

83. Sagnella S. Anderson E. Sanabria N. Marchant R.E. Kottke-Marchant K. Human endothelial cell interaction with biomimetic surfactant polymers containing peptide ligands from the heparin binding domain of fibronectin. Tissue Eng. 2005;11:226. DOI: 10.1089/ten.2005.11.226

84. Salacinski H.J. Tiwari A. Hamilton G. Seifalian A.M. Cellular engineering of vascular bypass grafts: role of chemical coatings for enhancing endothelial cell attachment. Med Biol Eng Comput. 2001;39:609. DOI: 10.1007/BF02345431

85. Hsu S.H. Tsai I.J. Lin D.J. Chen D.C. The effect of dynamic culture conditions on endothelial cell seeding and retention on small diameter polyurethane vascular grafts. Med Eng Phys. 2005;27:267. DOI: 10.1016/j.medengphy.2004.10.008

86. Williams C. Wick T.M. Perfusion bioreactor for small diameter tissue-engineered arteries. Tissue Eng. 2004;10:930. DOI: 10.1089/1076327041348536

87. Godbey W.T. Hindy S.B. Sherman M.E. Atala A. A novel use of centrifugal force for cell seeding into porous scaffolds. Biomaterials. 2004;25:2799.
DOI: 10.1016/j.biomaterials.2003.09.056

88. Vunjak-Novakovic G. Obradovic B. Martin I. Bursac P.M. Langer R. Freed L.E. Dynamic cell seeding of polymer scaffolds for cartilage tissue engineering. Biotechnol Prog. 1998;14:193
DOI: 10.1021/bp970120j

89. Nieponice A. Soletti L. Guan J. Deasy B.M. Huard J. Wagner W.R. Vorp D.A. Development of a tissue-engineered vascular graft combining a biodegradable scaffold, muscle-derived stem cells and a rotational vacuum seeding technique. Biomaterials. 2008;29:825.
DOI: 10.1016/j.biomaterials.2007.10.044

90. Tiwari A. Punshon G. Kidane A. Hamilton G. Seifalian A.M. Magnetic beads (Dynabead) toxicity to endothelial cells at high bead concentration: implication for tissue engineering of vascular prosthesis. Cell Biol Toxicol. 2003;19:265.
DOI: 10.1023/b:cbto.0000004929.37511.ed

91. Perea H. Aigner J. Hopfner U. Wintermantel E. Direct magnetic tubular cell seeding: a novel approach for vascular tissue engineering. Cells Tissues Organs. 2006;183:156.
DOI: 10.1159/000095989

92. Ito A. Hayashida M. Honda H. Hata K. Kagami H. Ueda M. Kobayashi T. Construction and harvest of multilayered keratinocyte sheets using magnetite nanoparticles and magnetic force. Tissue Eng. 2004;10:873. DOI: 10.1089/1076327041348446

93. Shimizu K. Ito A. Arinobe M. Murase Y. Iwata Y. Narita Y. Kagami H. Ueda M. Honda H. Effective cell-seeding technique using magnetite nanoparticles and magnetic force onto

decellularized blood vessels for vascular tissue engineering. J Biosci Bioeng. 2007;103:472. DOI: 10.1263/jbb.103.472

94. Bowlin G.L. Meyer A. Fields C. Cassano A. Makhoul R.G. Allen C. Rittgers S.E. The persistence of electrostatically seeded endothelial cells lining a small diameter expanded polytetrafluoroethylene vascular graft. J Biomater Appl. 2001;16:157. DOI: 10.1106/NCQT-JFV9-2EQ1-EBGU

95. Fields C. Cassano A. Allen C. Meyer A. Pawlowski K.J. Bowlin G.L. Rittgers S.E. Szycher M. Endothelial cell seeding of a 4-mm I.D. polyurethane vascular graft. J Biomater Appl. 2002;17:45. DOI: 10.1177/088532820201700186l

96. Topper J.N. Gimbrone M.A., Jr. Blood flow and vascular gene expression: fluid shear stress as a modulator of endothelial phenotype. Mol Med Today. 1999;5:40. DOI: 10.1016/s1357-4310(98)01372-0

97. Resnick N. Yahav H. Shay-Salit A. Shushy M. Schubert S. Zilberman L.C. Wofovitz E. Fluid shear stress and the vascular endothelium: for better and for worse. Prog Biophys Mol Biol. 2003;81:177. DOI: 10.1016/s0079-6107(02)00052-4

98. Meuleman N. Tondreau T. Delforge A. Dejeneffe M. Massy M. Libertalis M. Bron D. Lagneaux L. Human marrow mesenchymal stem cell culture: serum-free medium allows better expansion than classical alpha-MEM medium. Eur J Haematol. 2006;76:309. DOI: 10.1111/j.1600-0609.2005.00611.x

99. Chevallier N. Anagnostou F. Zilber S. Bodivit G. Maurin S. Barrault A. Bierling P. Hernigou P. Layrolle P. Rouard H. Osteoblastic differentiation of human mesenchymal stem cells with platelet lysate. Biomaterials. 2009;31:270. DOI: 10.1016/j.biomaterials.2009.09.043

100. Mann B.K. Gobin A.S. Tsai A.T. Schmedlen R.H. West J.L. Smooth muscle cell growth in photopolymerized hydrogels with cell adhesive and proteolytically degradable domains: synthetic ECM analogs for tissue engineering. Biomaterials. 2001;22:3045. DOI: 10.1016/s0142-9612(01)00051-5

101. Schmedlen R.H. Elbjeirami W.M. Gobin A.S. West J.L. Tissue engineered small-diameter vascular grafts. Clin Plast Surg. 2003;30:507. DOI: 10.1016/s0094-1298(03)00069-5

102. Sodian R. Lemke T. Fritsche C. Hoerstrup S.P. Fu P. Potapov E.V. Hausmann H. Hetzer R. Tissue-engineering bioreactors: a new combined cell-seeding and perfusion system for vascular tissue engineering. Tissue Eng. 2002;8:863. DOI: 10.1089/10763270260424222

103. Soletti L. Nieponice A. Guan J. Stankus J.J. Wagner W.R. Vorp D.A. A seeding device for tissue engineered tubular structures. Biomaterials. 2006;27:4863. DOI: 10.1016/j.biomaterials.2006.04.042

104. Fields, C., Cassano, A., Makhoul, R.G., Allen, C., Sims, R., Bulgrin, J., Meyer, A., Bowlin, G.L., and Rittgers, S.E. Evaluation of electrostatically endothelial cell seeded expanded

polytetrafluoroethylene grafts in a canine femoral artery model. J Biomater Appl 17, 135, 2002. DOI: 10.1106/088532802030556

8. List of figures

9. List of tables

10. Appendix

10.1. G-codes

10.1.1. G-codes for 20 degree of rotation angle and 1mm/s velocity

In this G-code cells will be seeded in 18 strip lines, while the operation velocity is considered 1mm/s for axial movement

M203 X50 Y50 Z50

G28

G04 P5000

G0 X5 Y20

G04 P2000

G0 A0 F60

G0 X72 Z1.2778 F60

G04 P2000

G0 A0.2 F60

G0 X5 Z2.5556 F60

G04 P2000

G0 A0.4 F60

G0 X72 Z3.8333 F60

G04 P2000

G0 A0.6 F60

G0 X5 Z5.1111 F60

G04 P2000

G0 A0.8 F60

G0 X72 Z6.3889 F60

G04 P2000

G0 A1 F60

G0 X5 Z7.6667 F60

G04 P2000

G0 A1.2 F60

G0 X72 Z8.9444 F60

G04 P2000

G0 A1.4 F60

G0 X5 Z10.2222 F60

G04 P2000

G0 A1.6 F60

G0 X72 Z11.5 F60

G04 P2000

G0 A1.8 F60

G0 X5 Z12.7778 F60

G04 P2000

G0 A2 F60

G0 X72 Z14.0556 F60

G04 P2000

G0 A2.2 F60

G0 X5 Z15.3333 F60

G04 P2000

G0 A2.4 F60

G0 X72 Z16.6111 F60

G04 P2000

G0 A2.6 F60

G0 X5 Z17.8889 F60

G04 P2000

G0 A2.8 F60

G0 X72 Z19.1667 F60

G04 P2000

G0 A3 F60

G0 X5 Z20.4444 F60

G04 P2000

G0 A3.2 F60

G0 X72 Z21.7222 F60

G04 P2000

G0 A3.4 F60

G0 X5 Z23 F60

G04 P2000

G28 X Y Z

M84